Available online at www.sciencedirect.com
ScienceDirect
Comput. Methods Appl. Mech. Engrg. 365 (2020) 113007
Computer methods in applied mechanics and engineering
www.elsevier.com/locate/cma

On an adaptive stabilized mixed finite element method for the Oseen problem with mixed boundary conditions

Tomás P. Barrios[a], J. Manuel Cascón[b], María González[c,*]

[a] Departamento de Matemática y Física Aplicadas, Universidad Católica de la Santísima Concepción, Casilla 297, Concepción, Chile
[b] Departamento de Economía e Historia Económica, Universidad de Salamanca, Salamanca, 37008, Spain
[c] Departamento de Matemáticas and CITIC, Universidade da Coruña, Campus de Elviña s/n, 15071, A Coruña, Spain

Received 26 July 2019; received in revised form 17 March 2020; accepted 17 March 2020
Available online xxxx

Abstract

We consider the Oseen problem with nonhomogeneous Dirichlet boundary conditions on a part of the boundary and a Neumann type boundary condition on the remaining part. Suitable least squares terms that arise from the constitutive law, the momentum equation and the Dirichlet boundary condition are added to a dual-mixed formulation based on the pseudostress-velocity variables. We prove that the new augmented variational formulation and the corresponding Galerkin scheme are well-posed, and a Céa estimate holds for any finite element subspaces. We also provide the rate of convergence when each row of the pseudostress is approximated by Raviart–Thomas elements and the velocity is approximated by continuous piecewise polynomials. We develop an a posteriori error analysis based on a Helmholtz-type decomposition, and derive a posteriori error indicators that consist of two residual terms per element except on those elements with a side on the Dirichlet boundary, where they both have two additional terms. We prove that these a posteriori error indicators are reliable and locally efficient. Finally, we provide several numerical experiments that support the theoretical results.

MSC: 65N30; 65N12; 65N15

Keywords: Oseen; Mixed finite element; Stabilization; A posteriori error estimates

1. Introduction

In the recent paper [1], we proposed and analyzed augmented mixed finite element methods for the Oseen problem in the pseudostress-velocity variables assuming homogeneous Dirichlet boundary conditions. That approach allows us to use any pair of conforming approximation spaces for the unknowns. Additionally, we partially followed [2] (see also [3]) and endowed that scheme with a simple a posteriori error indicator of residual type, which consists of just two residual terms per element, and is reliable and locally efficient. The corresponding adaptive mixed finite element method exhibits a good performance in numerical experiments.

Augmented formulations are often used to avoid the inf–sup condition in mixed finite element methods; cf., for instance, [1,3–8] and the references therein. In this paper, we consider the Oseen problem with nonhomogeneous

* Corresponding author.
E-mail addresses: tomas@ucsc.cl (T.P. Barrios), casbar@usal.es (J.M. Cascón), maria.gonzalez.taboada@udc.es (M. González).

https://doi.org/10.1016/j.cma.2020.113007

Dirichlet boundary conditions on a part of the boundary and a Neumann type boundary condition on the remaining part (which reduces to the so-called *do-nothing* boundary condition in the homogeneous case). We followed [1,9] and rewrite the problem in terms of the pseudostress and velocity variables. Then, we follow [1,6] and add suitable least squares terms to a dual-mixed formulation of the problem. The new augmented variational formulation and the corresponding Galerkin scheme are well-posed for appropriate values of the stabilization parameters, and a Céa estimate holds for any finite element subspaces. We also provide the rate of convergence when each row of the pseudostress is approximated by Raviart–Thomas elements and the velocity is approximated by continuous piecewise polynomials. Moreover, we develop an a posteriori error analysis based on a quasi-Helmholtz decomposition [10,11] in two dimensions and a Helmholtz decomposition in three dimensions [12], and derive in each case an a posteriori error indicator that consists of two residual terms per element except on elements with a side on the Dirichlet boundary, where it has two additional terms. These a posteriori error indicators are proved to be reliable and locally efficient. Finally, we provide several numerical experiments that support the theoretical results. More precisely, we first use the Kovasznay flow to confirm the theoretical convergence rates predicted by the theory. Then, we test an adaptive algorithm based on the new a posteriori error indicator over a non-convex domain and a domain with a crack. We end with the solution of a three-dimensional Oseen problem with mixed boundary conditions.

The paper is organized as follows. In Section 2 we describe the model problem and its formulation in terms of the pseudostress and velocity variables. In Section 3 we introduce and analyze an augmented dual-mixed variational formulation of the problem. Then, in Section 4 we analyze the corresponding Galerkin scheme and establish optimal error estimates for stabilized mixed finite element methods based on the approximation of the pseudostress by Raviart–Thomas elements and that of the velocity by continuous piecewise polynomials. Section 5 is devoted to the a posteriori error analysis of the augmented mixed finite element method. Finally, some numerical experiments are reported in Section 6 and some conclusions are drawn in Section 7.

We end this section with some notations to be used throughout the paper. Let $d = 2$ or 3. Given any Hilbert space H, we denote by H^d the space of vectors of order d with entries in H, and by $H^{d\times d}$ the space of square tensors of order d with entries in H. Let $\mathbf{I}$ be the identity matrix in $\mathbb{R}^{d\times d}$. Given $\boldsymbol{\tau} := (\tau_{ij})$, $\boldsymbol{\zeta} := (\zeta_{ij}) \in \mathbb{R}^{d\times d}$, we write, as usual, $\boldsymbol{\tau}^{\mathtt{t}} := (\tau_{ji})$, $\mathrm{tr}(\boldsymbol{\tau}) := \sum_{i=1}^{d} \tau_{ii}$, $\boldsymbol{\tau}^{\mathtt{d}} := \boldsymbol{\tau} - \frac{1}{d}\mathrm{tr}(\boldsymbol{\tau})\mathbf{I}$ and $\boldsymbol{\tau} : \boldsymbol{\zeta} := \sum_{i,j=1}^{d} \tau_{ij}\,\zeta_{ij}$. Throughout this paper, we will use the standard notations for Sobolev spaces and norms. If Ω is a bounded connected set in $\mathbb{R}^d$, with a Lipschitz-continuous boundary Γ, we denote $H(\mathrm{div},\Omega) := \{\mathbf{v} \in [L^2(\Omega)]^d : \mathrm{div}(\mathbf{v}) \in L^2(\Omega)\}$ endowed with the norm $\|\mathbf{v}\|_{H(\mathrm{div},\Omega)} := (\|\mathbf{v}\|^2_{[L^2(\Omega)]^d} + \|\mathrm{div}(\mathbf{v})\|^2_{L^2(\Omega)})^{1/2}$, and $H(\mathbf{div},\Omega) := \{\boldsymbol{\tau} \in [L^2(\Omega)]^{d\times d} : \mathbf{div}(\boldsymbol{\tau}) \in [L^2(\Omega)]^d\}$, endowed with the norm $\|\boldsymbol{\tau}\|_{H(\mathbf{div},\Omega)} := (\|\boldsymbol{\tau}\|^2_{[L^2(\Omega)]^{d\times d}} + \|\mathbf{div}(\boldsymbol{\tau})\|^2_{[L^2(\Omega)]^d})^{1/2}$.

2. A pseudostress-velocity formulation of the Oseen problem

Let Ω be a bounded connected open set in $\mathbb{R}^d$ ($d = 2$ or 3), with a Lipschitz-continuous boundary Γ. We assume that $\Gamma = \overline{\Gamma}_D \cup \overline{\Gamma}_N$, where Γ_D is a closed connected part of Γ and $\Gamma_N = \Gamma \setminus \Gamma_D$. We assume that both Γ_D and Γ_N have positive measure. Let us consider an incompressible fluid that occupies the region Ω. Let $\nu > 0$ be the kinematic viscosity of the fluid, that we assume constant. We denote by $\mathbf{a} \in [L^\infty(\Omega)]^d$, $\mathbf{a} \neq \mathbf{0}$, the advective velocity field, assumed to be solenoidal in Ω and such that $\mathbf{a}\cdot\mathbf{n} \geq 0$ on Γ_N, where $\mathbf{n}$ denotes the unit outward normal vector to Γ_N. Let $\mathbf{f} \in [L^2(\Omega)]^d$ be an external body force, $\mathbf{u}_D \in [H^{1/2}(\Gamma_D)]^d$ be a prescribed velocity on the Dirichlet boundary Γ_D and $\mathbf{g} \in [H^{-1/2}(\Gamma_N)]^d$ be the Neumann data. We consider the following Oseen problem: find the velocity field $\mathbf{u}$ and the pressure p such that

$$\left\{\begin{array}{rcll} -\nu\Delta\mathbf{u} + \mathbf{a}\cdot\nabla\mathbf{u} + \nabla p &=& \mathbf{f} & \text{in } \Omega, \\ \mathrm{div}(\mathbf{u}) &=& 0 & \text{in } \Omega, \\ \mathbf{u} &=& \mathbf{u}_D & \text{on } \Gamma_D, \\ -p\mathbf{n} + \nu\dfrac{\partial\mathbf{u}}{\partial\mathbf{n}} &=& \mathbf{g} & \text{on } \Gamma_N. \end{array}\right. \tag{1}$$

Now, we follow [9] and define the pseudostress $\boldsymbol{\sigma} := \nu\nabla\mathbf{u} - p\,\mathbf{I}$. Then, problem (1) can be stated as follows: find $\boldsymbol{\sigma}$ and $\mathbf{u}$ such that

$$\left\{\begin{array}{rcll} -\mathbf{div}(\boldsymbol{\sigma}) + \mathbf{a}\cdot\nabla\mathbf{u} &=& \mathbf{f} & \text{in } \Omega, \\ \dfrac{1}{\nu}\boldsymbol{\sigma}^{\mathtt{d}} &=& \nabla\mathbf{u} & \text{in } \Omega, \\ \mathbf{u} &=& \mathbf{u}_D & \text{on } \Gamma_D, \\ \boldsymbol{\sigma}\mathbf{n} &=& \mathbf{g} & \text{on } \Gamma_N. \end{array}\right. \tag{2}$$

It is easy to verify that problem (2) is equivalent to problem (1) in the sense of the following Theorem.

Theorem 1. *If* $(\mathbf{u}, p)$ *is a solution to problem* (1)*, then* $(\boldsymbol{\sigma}, \mathbf{u})$*, where* $\boldsymbol{\sigma} = \nu \nabla \mathbf{u} - p\,\mathbf{I}$*, is a solution to problem* (2)*. Conversely, if* $(\boldsymbol{\sigma}, \mathbf{u})$ *is a solution to problem* (2)*, then* $(\mathbf{u}, p)$*, where* $p = -\frac{1}{d}\,\mathrm{tr}(\boldsymbol{\sigma})$*, is a solution to problem* (1)*.*

In particular, it is possible to recover the pressure p from the pseudostress through a simple post-processing.

Now, let $\boldsymbol{\sigma}_{\mathbf{g}}$ be such that $\boldsymbol{\sigma}_{\mathbf{g}}\mathbf{n} = \mathbf{g}$ on Γ_N. Then, we can write $\boldsymbol{\sigma} = \boldsymbol{\sigma}_{\mathbf{0}} + \boldsymbol{\sigma}_{\mathbf{g}}$, with $\boldsymbol{\sigma}_{\mathbf{0}}\mathbf{n} = \mathbf{0}$ on Γ_N. We remark that problem (2) is equivalent to the following problem:

$$\left\{\begin{array}{rcll} -\mathbf{div}(\boldsymbol{\sigma}_{\mathbf{0}}) + \mathbf{a}\cdot\nabla\mathbf{u} & = & \tilde{\mathbf{f}} & \text{in } \Omega\,, \\ \dfrac{1}{\nu}\,\boldsymbol{\sigma}_{\mathbf{0}}^{\mathtt{d}} & = & \nabla\mathbf{u} + \boldsymbol{\zeta} & \text{in } \Omega\,, \\ \mathbf{u} & = & \mathbf{u}_D & \text{on } \Gamma_D\,, \\ \boldsymbol{\sigma}_{\mathbf{0}}\mathbf{n} & = & \mathbf{0} & \text{on } \Gamma_N\,, \end{array}\right. \tag{3}$$

where $\tilde{\mathbf{f}} := \mathbf{f} + \mathbf{div}(\boldsymbol{\sigma}_{\mathbf{g}})$ and $\boldsymbol{\zeta} := -\frac{1}{\nu}\boldsymbol{\sigma}_{\mathbf{g}}^{\mathtt{d}}$. We remark that it can be shown that the solution of the original problem does not depend on the choice of $\boldsymbol{\sigma}_{\mathbf{g}}$.

Proceeding as usual, we arrive at the following dual-mixed variational formulation of problem (3): find $\boldsymbol{\sigma}_{\mathbf{0}} \in \mathbf{H}_{\mathbf{0}} := \{\boldsymbol{\tau} \in H(\mathbf{div}, \Omega) : \boldsymbol{\tau}\mathbf{n} = \mathbf{0} \quad \text{on } \Gamma_N\}$ and $\mathbf{u} \in [H^1(\Omega)]^d$ such that

$$\left\{\begin{array}{rcll} \dfrac{1}{\nu}\displaystyle\int_\Omega \boldsymbol{\sigma}_{\mathbf{0}}^{\mathtt{d}} : \boldsymbol{\tau}^{\mathtt{d}} + \int_\Omega \mathbf{u}\cdot\mathbf{div}(\boldsymbol{\tau}) & = & \displaystyle\int_\Omega \boldsymbol{\zeta} : \boldsymbol{\tau} + \int_{\Gamma_D} \mathbf{u}_D\cdot\boldsymbol{\tau}\mathbf{n}\,, & \forall\,\boldsymbol{\tau} \in \mathbf{H}_{\mathbf{0}}\,, \\ \displaystyle\int_\Omega \mathbf{div}(\boldsymbol{\sigma}_{\mathbf{0}})\cdot\mathbf{v} - \int_\Omega (\mathbf{a}\cdot\nabla\mathbf{u})\cdot\mathbf{v} & = & -\displaystyle\int_\Omega \tilde{\mathbf{f}}\cdot\mathbf{v}\,, & \forall\,\mathbf{v} \in [H^1(\Omega)]^d\,. \end{array}\right. \tag{4}$$

Let us define the bilinear forms $a : \mathbf{H}_{\mathbf{0}}\times\mathbf{H}_{\mathbf{0}} \to \mathbb{R}$, $b : [H^1(\Omega)]^d \times \mathbf{H}_{\mathbf{0}} \to \mathbb{R}$ and $c : [H^1(\Omega)]^d \times [H^1(\Omega)]^d \to \mathbb{R}$ as follows:

$$a(\boldsymbol{\sigma}, \boldsymbol{\tau}) := \frac{1}{\nu}\int_\Omega \boldsymbol{\sigma}^{\mathtt{d}} : \boldsymbol{\tau}^{\mathtt{d}}\,, \qquad b(\mathbf{u}, \boldsymbol{\tau}) := \int_\Omega \mathbf{u}\cdot\mathbf{div}(\boldsymbol{\tau})\,, \qquad c(\mathbf{u}, \mathbf{v}) := \int_\Omega (\mathbf{a}\cdot\nabla\mathbf{u})\cdot\mathbf{v},$$

for any $\boldsymbol{\sigma}, \boldsymbol{\tau} \in \mathbf{H}_0$ and $\mathbf{u}, \mathbf{v} \in [H^1(\Omega)]^d$. We also define the linear functionals $m : \mathbf{H}_{\mathbf{0}} \to \mathbb{R}$ by $m(\boldsymbol{\tau}) := \int_\Omega \boldsymbol{\zeta} : \boldsymbol{\tau} + \int_{\Gamma_D} \mathbf{u}_D\cdot\boldsymbol{\tau}\mathbf{n}$, $\forall\,\boldsymbol{\tau} \in \mathbf{H}_{\mathbf{0}}$ and $l : [L^2(\Omega)]^d \to \mathbb{R}$ by $l(\mathbf{v}) := -\int_\Omega \tilde{\mathbf{f}}\cdot\mathbf{v}$, $\forall\,\mathbf{v} \in [L^2(\Omega)]^d$. Then, the dual-mixed variational formulation (4) can be written in the form: find $\boldsymbol{\sigma}_{\mathbf{0}} \in \mathbf{H}_{\mathbf{0}}$ and $\mathbf{u} \in [H^1(\Omega)]^d$ such that

$$\left\{\begin{array}{rcll} a(\boldsymbol{\sigma}_{\mathbf{0}}, \boldsymbol{\tau}) + b(\mathbf{u}, \boldsymbol{\tau}) & = & m(\boldsymbol{\tau})\,, & \forall\,\boldsymbol{\tau} \in \mathbf{H}_{\mathbf{0}}\,, \\ b(\mathbf{v}, \boldsymbol{\sigma}_{\mathbf{0}}) - c(\mathbf{u}, \mathbf{v}) & = & l(\mathbf{v})\,, & \forall\,\mathbf{v} \in [H^1(\Omega)]^d\,, \end{array}\right. \tag{5}$$

which reflects the generalized saddle-point structure of the problem.

Since the bilinear form $c(\cdot,\cdot)$ is not symmetric, according to [13], sufficient conditions to ensure that problem (5) has a unique solution include that the bilinear form $a(\cdot,\cdot)$ be elliptic on $\mathbf{H}_{\mathbf{0}}$ and the bilinear form $b(\cdot,\cdot)$ satisfy an inf–sup condition in $\mathbf{H}_{\mathbf{0}}\times[H^1(\Omega)]^d$. However, it is well-known that $a(\cdot,\cdot)$ is elliptic in the divergence free subspace of $\mathbf{H}_{\mathbf{0}}$ (see, for instance, the proof of Theorem 2.3 in [9]) but not on $\mathbf{H}_{\mathbf{0}}$. These facts motivated us to consider an augmented formulation of problem (2).

3. Augmented dual-mixed variational formulation

In this section, we introduce and analyze an augmented variational formulation of problem (2). We combine ideas from [1] and [6] and subtract the second equation in (5) from the first one and then, add the following least-squares type terms, that arise from the momentum and constitutive equations in (3) and from the Dirichlet boundary condition:

$$\kappa_1 \int_\Omega (\mathbf{div}(\boldsymbol{\sigma}_{\mathbf{0}}) - \mathbf{a}\cdot\nabla\mathbf{u})\cdot(\mathbf{div}(\boldsymbol{\tau}) + \mathbf{a}\cdot\nabla\mathbf{v}) = -\kappa_1 \int_\Omega \tilde{\mathbf{f}}\cdot(\mathbf{div}(\boldsymbol{\tau}) + \mathbf{a}\cdot\nabla\mathbf{v}) \tag{6}$$

$$\kappa_2 \int_\Omega (\nabla\mathbf{u} - \frac{1}{\nu}\,\boldsymbol{\sigma}_{\mathbf{0}}^{\mathtt{d}}) : (\nabla\mathbf{v} + \frac{1}{\nu}\,\boldsymbol{\tau}^{\mathtt{d}}) = -\kappa_2 \int_\Omega \boldsymbol{\zeta} : (\nabla\mathbf{v} + \frac{1}{\nu}\boldsymbol{\tau}^{\mathtt{d}})\,, \tag{7}$$

and

$$\kappa_3 \int_{\Gamma_D} \mathbf{u}\cdot\mathbf{v} = \kappa_3 \int_{\Gamma_D} \mathbf{u}_D\cdot\mathbf{v}\,, \tag{8}$$

where $(\boldsymbol{\sigma_0}, \mathbf{u}) \in \mathbf{H_0} \times [H^1(\Omega)]^d$ is the solution of (3) and $(\boldsymbol{\tau}, \mathbf{v}) \in \mathbf{H_0} \times [H^1(\Omega)]^d$ is a test function. The stabilization parameters, κ_1, κ_2 and κ_3, are positive constants to be chosen so that the augmented bilinear form

$$A((\boldsymbol{\sigma}, \mathbf{u}), (\boldsymbol{\tau}, \mathbf{v})) := \frac{1}{\nu}\int_\Omega \boldsymbol{\sigma}^{\mathtt{d}} : \boldsymbol{\tau}^{\mathtt{d}} + \int_\Omega \mathbf{u}\cdot\mathbf{div}(\boldsymbol{\tau}) - \int_\Omega \mathbf{div}(\boldsymbol{\sigma})\cdot\mathbf{v} + \int_\Omega (\mathbf{a}\cdot\nabla\mathbf{u})\cdot\mathbf{v}$$
$$+\kappa_1\int_\Omega (\mathbf{div}(\boldsymbol{\sigma}) - \mathbf{a}\cdot\nabla\mathbf{u})\cdot(\mathbf{div}(\boldsymbol{\tau}) + \mathbf{a}\cdot\nabla\mathbf{v}) + \kappa_2\int_\Omega (\nabla\mathbf{u} - \frac{1}{\nu}\boldsymbol{\sigma}^{\mathtt{d}}) : (\nabla\mathbf{v} + \frac{1}{\nu}\boldsymbol{\tau}^{\mathtt{d}}) + \kappa_3\int_{\Gamma_D}\mathbf{u}\cdot\mathbf{v}$$

is elliptic in the whole space $\mathbf{H_0} \times [H^1(\Omega)]^d$.

Let us define the augmented linear functional $F : \mathbf{H_0} \times [H^1(\Omega)]^d \to \mathbb{R}$ by

$$\begin{aligned} F(\boldsymbol{\tau}, \mathbf{v}) \;:=\; & \int_\Omega \boldsymbol{\zeta} : \boldsymbol{\tau} + \int_{\Gamma_D} \mathbf{u}_D\cdot\boldsymbol{\tau}\mathbf{n} + \int_\Omega \tilde{\mathbf{f}}\cdot\mathbf{v} - \kappa_1\int_\Omega \tilde{\mathbf{f}}\cdot(\mathbf{div}(\boldsymbol{\tau}) + \mathbf{a}\cdot\nabla\mathbf{v}) \\ - \;& \kappa_2\int_\Omega \boldsymbol{\zeta} : (\nabla\mathbf{v} + \frac{1}{\nu}\boldsymbol{\tau}^{\mathtt{d}}) + \kappa_3\int_{\Gamma_D}\mathbf{u}_D\cdot\mathbf{v}\,, \qquad \forall\,(\boldsymbol{\tau}, \mathbf{v}) \in \mathbf{H_0}\times[H^1(\Omega)]^d\,. \end{aligned}$$

Then, the augmented variational formulation of problem (3) reads: find $(\boldsymbol{\sigma_0}, \mathbf{u}) \in \mathbf{H_0} \times [H^1(\Omega)]^d$ such that

$$A((\boldsymbol{\sigma_0}, \mathbf{u}), (\boldsymbol{\tau}, \mathbf{v})) = F(\boldsymbol{\tau}, \mathbf{v})\,, \qquad \forall\,(\boldsymbol{\tau}, \mathbf{v}) \in \mathbf{H_0}\times[H^1(\Omega)]^d\,. \tag{9}$$

It is important to remark that in case of homogeneous Dirichlet boundary conditions, that is, when $\Gamma_D = \Gamma$, $\Gamma_N = \emptyset$ and $\mathbf{u}_D = \mathbf{0}$ on Γ_D, we obtain the same linear functional F as in [1]; however, the variational formulation is not equivalent, since here we look for $\mathbf{u} \in [H^1(\Omega)]^d$ instead of $[H^1_0(\Omega)]^d$. This is because in [1], we imposed the Dirichlet boundary condition in a strong sense, whereas here we do it weakly.

The following two Lemmas will be used to prove the ellipticity of $A(\cdot,\cdot)$ in $\mathbf{H_0} \times [H^1(\Omega)]^d$.

Lemma 1. *There exists a positive constant c_1, which depends only on Ω, such that*

$$c_1\,\|\boldsymbol{\tau}\|^2_{[L^2(\Omega)]^{d\times d}} \;\le\; \|\boldsymbol{\tau}^{\mathtt{d}}\|^2_{[L^2(\Omega)]^{d\times d}} + \|\mathbf{div}(\boldsymbol{\tau})\|^2_{[L^2(\Omega)]^d}\,, \quad \forall\,\boldsymbol{\tau} \in \mathbf{H}_0.$$

Proof. See Lemma 3.1 in [14] or Proposition 3.1, Chapter IV of [13]. □

Lemma 2. *There exists a positive constant c_2, which depends only on Ω, such that*

$$\|\nabla\mathbf{v}\|^2_{[L^2(\Omega)]^{d\times d}} + \|\mathbf{v}\|^2_{[L^2(\Gamma_D)]^d} \;\ge\; c_2\,\|\mathbf{v}\|^2_{[H^1(\Omega)]^d}\,, \qquad \forall\,\mathbf{v} \in [H^1(\Omega)]^d.$$

Proof. It is similar to the proof of Lemma 3.3 in [5]. □

Next, we prove the ellipticity of $A(\cdot,\cdot)$ in $\mathbf{H_0} \times [H^1(\Omega)]^d$ under some conditions on the stabilization parameters.

Lemma 3. *Assume that*

$$0 < \kappa_1 < \frac{\kappa_2}{d\,\|\mathbf{a}\|^2_{[L^\infty(\Omega)]^d}}\,, \qquad 0 < \kappa_2 < \nu\,, \qquad \textit{and} \qquad \kappa_3 > \frac{1}{2}\,\|\mathbf{a}\cdot\mathbf{n}\|_{L^\infty(\Gamma_D)}.$$

Then, there exists $C_{\mathtt{ell}} > 0$ such that

$$A((\boldsymbol{\tau}, \mathbf{v}), (\boldsymbol{\tau}, \mathbf{v})) \ge C_{\mathtt{ell}}\,\|(\boldsymbol{\tau}, \mathbf{v})\|^2_{\mathbf{H_0}\times[H^1(\Omega)]^d}\,, \quad \forall\,(\boldsymbol{\tau}, \mathbf{v}) \in \mathbf{H_0}\times[H^1(\Omega)]^d.$$

Proof. Let $(\boldsymbol{\tau}, \mathbf{v}) \in \mathbf{H_0} \times [H^1(\Omega)]^d$. Then, using the definition of $A(\cdot,\cdot)$, we have

$$\begin{aligned} A((\boldsymbol{\tau}, \mathbf{v}), (\boldsymbol{\tau}, \mathbf{v})) \;=\; & \frac{1}{\nu}\left(1 - \frac{1}{\nu}\kappa_2\right)\|\boldsymbol{\tau}^{\mathtt{d}}\|^2_{[L^2(\Omega)]^{d\times d}} + \int_\Omega (\mathbf{a}\cdot\nabla\mathbf{v})\cdot\mathbf{v} + \kappa_1\,\|\mathbf{div}(\boldsymbol{\tau})\|^2_{[L^2(\Omega)]^d} \\ - \;& \kappa_1\,\|\mathbf{a}\cdot\nabla\mathbf{v}\|^2_{[L^2(\Omega)]^d} + \kappa_2\,\|\nabla\mathbf{v}\|^2_{[L^2(\Omega)]^{d\times d}} + \kappa_3\,\|\mathbf{v}\|^2_{[L^2(\Gamma_D)]^d} \end{aligned}$$

We remark that, since $\mathbf{a}$ is solenoidal, using that $\mathbf{a}\cdot\mathbf{n} \ge 0$ on Γ_N, we have

$$\int_\Omega (\mathbf{a}\cdot\nabla\mathbf{v})\cdot\mathbf{v} = \frac{1}{2}\int_\Gamma |\mathbf{v}|^2\mathbf{a}\cdot\mathbf{n} \ge \frac{1}{2}\int_{\Gamma_D} |\mathbf{v}|^2\mathbf{a}\cdot\mathbf{n} \ge -\frac{1}{2}\|\mathbf{a}\cdot\mathbf{n}\|_{L^\infty(\Gamma_D)}\|\mathbf{v}\|^2_{[L^2(\Gamma_D)]^d}.$$

On the other hand,

$$\|\mathbf{a}\cdot\nabla\mathbf{v}\|^2_{[L^2(\Omega)]^d} \leq d\,\|\mathbf{a}\|^2_{[L^\infty(\Omega)]^d}\,\|\nabla\mathbf{v}\|^2_{[L^2(\Omega)]^{d\times d}}.$$

Therefore,

$$\begin{aligned} A((\boldsymbol{\tau},\mathbf{v}),(\boldsymbol{\tau},\mathbf{v})) &\geq \frac{1}{\nu}\left(1-\frac{\kappa_2}{\nu}\right)\left\|\boldsymbol{\tau}^{\mathtt{d}}\right\|^2_{[L^2(\Omega)]^{d\times d}} + \kappa_1\,\|\mathbf{div}(\boldsymbol{\tau})\|^2_{[L^2(\Omega)]^d} \\ &+ \left(\kappa_2 - d\,\kappa_1\,\|\mathbf{a}\|^2_{[L^\infty(\Omega)]^d}\right)\|\nabla\mathbf{v}\|^2_{[L^2(\Omega)]^{d\times d}} + (\kappa_3-\frac{1}{2}\|\mathbf{a}\cdot\mathbf{n}\|_{L^\infty(\Gamma_D)})\,\|\mathbf{v}\|^2_{[L^2(\Gamma_D)]^d}. \end{aligned}$$

Then, by applying Lemmas 1 and 2, the ellipticity of $A(\cdot,\cdot)$ follows for the feasible values of κ_1, κ_2 and κ_3, with

$$C_{\mathtt{ell}} = \min(\frac{1}{\nu}\left(1-\frac{\kappa_2}{\nu}\right)c_1,\ \frac{\kappa_1}{2}c_1,\ \frac{\kappa_1}{2},\ \left(\kappa_2-\kappa_1\,d\,\|\mathbf{a}\|^2_{[L^\infty(\Omega)]^2}\right)c_2,\ (\kappa_3-\frac{1}{2}\|\mathbf{a}\cdot\mathbf{n}\|_{L^\infty(\Gamma_D)})\,c_2). \quad \square$$

Remark. We recall that we assumed $\mathbf{a}\neq\mathbf{0}$. In case $\mathbf{a}=\mathbf{0}$, we would be dealing with the Stokes problem. In this case,

$$C_{\mathtt{ell}} = \min(\frac{1}{\nu}\left(1-\frac{\kappa_2}{\nu}\right)c_1,\ \frac{\kappa_1}{2}c_1,\ \frac{\kappa_1}{2},\ \kappa_2\,c_2,\ \kappa_3\,c_2),$$

so that the values of the stabilization parameters that guarantee the ellipticity of the augmented bilinear form $A(\cdot,\cdot)$ are

$$\kappa_1>0\,,\qquad \kappa_2\in(0,\nu)\,,\qquad \kappa_3>0. \quad \square$$

Theorem 2. *Assume the hypotheses of Lemma 3. Then, problem (9) has a unique solution* $(\boldsymbol{\sigma}_{\mathbf{0}},\mathbf{u})\in\mathbf{H}_{\mathbf{0}}\times[H^1(\Omega)]^d$ *and there holds*

$$\|(\boldsymbol{\sigma}_{\mathbf{0}},\mathbf{u})\|_{\mathbf{H}_{\mathbf{0}}\times[H^1(\Omega)]^d} \leq C^{-1}_{\mathtt{ell}}\,M\,(\|\mathbf{f}\|_{[L^2(\Omega)]^d} + \|\mathbf{u}_D\|_{[H^{1/2}(\Gamma_D)]^d} + \|\boldsymbol{\sigma}_{\mathbf{g}}\|_{H(\mathbf{div};\Omega)}),$$

where $M := \max(1+\kappa_1\,(1+\sqrt{d}\,\|\mathbf{a}\|_{[L^\infty(\Omega)]^d}),\ \frac{1}{\nu}(1+\kappa_2(1+\frac{1}{\nu})),\ 1+\kappa_3)$.

Proof. From Lemma 3, the augmented continuous bilinear form $A(\cdot,\cdot)$ is elliptic in $\mathbf{H}_{\mathbf{0}}\times[H^1(\Omega)]^d$. On the other hand, the augmented linear functional F is continuous in $\mathbf{H}_{\mathbf{0}}\times[H^1(\Omega)]^d$, with

$$|F(\boldsymbol{\tau},\mathbf{v})| \leq M\,(\|\mathbf{f}\|_{[L^2(\Omega)]^d} + \|\mathbf{u}_D\|_{[H^{1/2}(\Gamma_D)]^d} + \|\boldsymbol{\sigma}_{\mathbf{g}}\|_{H(\mathbf{div};\Omega)})\,\|(\boldsymbol{\tau},\mathbf{v})\|_{\mathbf{H}_{\mathbf{0}}\times[H^1(\Omega)]^d}.$$

Then, the result follows by applying the Lax–Milgram Lemma. $\square$

4. Augmented mixed finite element method

In what follows, we assume that Ω is a polygonal or polyhedral domain. Let $\{\mathcal{T}_h\}_{h>0}$ be a family of shape-regular meshes of $\bar{\Omega}$ made up of triangles if $d=2$ or tetrahedra if $d=3$. We denote by h_T the diameter of an element $T\in\mathcal{T}_h$ and define $h := \max_{T\in\mathcal{T}_h} h_T$. Let $\mathbf{H}_{\mathbf{0},h}$ and $\mathbf{V}_h$ be any finite element subspaces of $\mathbf{H}_{\mathbf{0}}$ and $[H^1(\Omega)]^d$, respectively. Then, the Galerkin scheme associated to problem (9) reads: find $(\boldsymbol{\sigma}_{\mathbf{0},h},\mathbf{u}_h)\in\mathbf{H}_{\mathbf{0},h}\times\mathbf{V}_h$ such that

$$A((\boldsymbol{\sigma}_{\mathbf{0},h},\mathbf{u}_h),(\boldsymbol{\tau}_h,\mathbf{v}_h)) = F(\boldsymbol{\tau}_h,\mathbf{v}_h)\,,\qquad \forall\,(\boldsymbol{\tau}_h,\mathbf{v}_h)\in\mathbf{H}_{\mathbf{0},h}\times\mathbf{V}_h\,. \tag{10}$$

Under the hypotheses of Lemma 3, the bilinear form $A(\cdot,\cdot)$ is elliptic in $\mathbf{H}_{\mathbf{0}}\times[H^1(\Omega)]^d$, and hence, $A(\cdot,\cdot)$ is elliptic in any finite element subspace $\mathbf{H}_{\mathbf{0},h}\times\mathbf{V}_h$ of $\mathbf{H}_{\mathbf{0}}\times[H^1(\Omega)]^d$. Therefore, problem (10) has a unique solution $(\boldsymbol{\sigma}_{\mathbf{0},h},\mathbf{u}_h)\in\mathbf{H}_{\mathbf{0},h}\times\mathbf{V}_h$. Moreover, there exists a constant $C_{\mathtt{Cea}}>0$, independent of h, such that

$$\|(\boldsymbol{\sigma}_{\mathbf{0}}-\boldsymbol{\sigma}_{\mathbf{0},h},\mathbf{u}-\mathbf{u}_h)\|_{\mathbf{H}_{\mathbf{0}}\times[H^1(\Omega)]^d} \leq C_{\mathtt{Cea}}\inf_{(\boldsymbol{\tau}_h,\mathbf{v}_h)\in\mathbf{H}_{\mathbf{0},h}\times\mathbf{V}_h}\|(\boldsymbol{\sigma}_{\mathbf{0}}-\boldsymbol{\tau}_h,\mathbf{u}-\mathbf{v}_h)\|_{\mathbf{H}_{\mathbf{0}}\times[H^1(\Omega)]^d}\,. \tag{11}$$

In order to establish a rate of convergence result, we consider specific finite element subspaces $\mathbf{H}_{\mathbf{0},h}$ and $\mathbf{V}_h$. Hereafter, given $T\in\mathcal{T}_h$ and an integer $l\geq 0$, we denote by $\mathcal{P}_l(T)$ the space of polynomials of total degree at most l on T and, given an integer $k\geq 0$, we denote by $\mathcal{RT}_k(T)$ the local Raviart–Thomas–Nédélec space of order $k+1$

(cf. [15]),

$$\mathcal{RT}_k(T) := [\mathcal{P}_k(T)]^d \oplus [\mathbf{x}]\mathcal{P}_k(T) \subset [\mathcal{P}_{k+1}(T)]^d,$$

where $\mathbf{x}$ is a generic vector of $\mathbb{R}^d$.

Let $k \geq 0$ and $m \geq 1$. Then, we let $\mathbf{H}_{\mathbf{0},h}$ be the Raviart–Thomas–Nédélec space

$$\mathbf{H}_{\mathbf{0},h} := \Big\{ \boldsymbol{\tau}_h \in \mathbf{H}_0 \,:\, \boldsymbol{\tau}_h\big|_T \in [\mathcal{RT}_k(T)^{\mathtt{t}}]^d, \quad \forall\, T \in \mathcal{T}_h \Big\},$$

and we define

$$\mathbf{V}_h := [\mathcal{L}_m]^d = \Big\{ \mathbf{v}_h \in [\mathcal{C}(\overline{\Omega})]^d \,:\, \mathbf{v}_h\big|_T \in [\mathcal{P}_m(T)]^d, \quad \forall\, T \in \mathcal{T}_h \Big\}.$$

In what follows, we assume that $\mathbf{g}$ is componentwise a piecewise polynomial of degree at most k over the initial mesh, so that we can choose $\boldsymbol{\sigma}_{\mathbf{g}}$ in the Raviart–Thomas space of order k. The corresponding rate of convergence is given in the next Theorem.

Theorem 3. *Assume $\boldsymbol{\sigma}_{\mathbf{0}} \in [H^t(\Omega)]^{d\times d}$, $\mathbf{div}(\boldsymbol{\sigma}_{\mathbf{0}}) \in [H^t(\Omega)]^d$ and $\mathbf{u} \in [H^{t+1}(\Omega)]^d$. Then, under the assumptions of Lemma 3, there exists $C = \mathcal{O}(C_{\mathtt{Cea}}) > 0$, independent of h, such that*

$$\|(\boldsymbol{\sigma}_{\mathbf{0}} - \boldsymbol{\sigma}_{\mathbf{0},h}, \mathbf{u} - \mathbf{u}_h)\|_{\mathbf{H}_{\mathbf{0}}\times[H^1(\Omega)]^d} \,\leq\, C\, h^{\beta}\Big(\|\boldsymbol{\sigma}_{\mathbf{0}}\|_{[H^t(\Omega)]^{d\times d}} + \|\mathbf{div}(\boldsymbol{\sigma}_{\mathbf{0}})\|_{[H^t(\Omega)]^d} + \|\mathbf{u}\|_{[H^{t+1}(\Omega)]^d} \Big), \tag{12}$$

where $\beta := \min\{t, m, k+1\}$.

Proof. It follows straightforwardly from inequality (11) and the approximation properties of the corresponding finite element subspaces. □

We remark that, by taking $p_h = -\frac{1}{d}\mathrm{tr}(\boldsymbol{\sigma}_{\mathbf{0},h} + \boldsymbol{\sigma}_{\mathbf{g}})$, under the hypothesis of the previous Theorem, we have that

$$\|p - p_h\|_{L^2(\Omega)} \,\leq\, C\, h^{\beta}\Big(\|\boldsymbol{\sigma}_{\mathbf{0}}\|_{[H^t(\Omega)]^{d\times d}} + \|\mathbf{div}(\boldsymbol{\sigma}_{\mathbf{0}})\|_{[H^t(\Omega)]^d} + \|\mathbf{u}\|_{[H^{t+1}(\Omega)]^d} \Big), \tag{13}$$

where $C = \mathcal{O}(C_{\mathtt{Cea}})$.

5. Residual-based a posteriori error analysis

In this section we develop an a posteriori error analysis of residual type in two and in three dimensions. Let us define the residual:

$$R(\boldsymbol{\tau}, \mathbf{v}) := F(\boldsymbol{\tau}, \mathbf{v}) - A((\boldsymbol{\sigma}_{\mathbf{0},h}, \mathbf{u}_h), (\boldsymbol{\tau}, \mathbf{v})), \tag{14}$$

where $(\boldsymbol{\sigma}_{\mathbf{0},h}, \mathbf{u}_h)$ is the solution of the augmented discrete problem (10). Since $(\boldsymbol{\sigma}_{\mathbf{0}} - \boldsymbol{\sigma}_{\mathbf{0},h}, \mathbf{u} - \mathbf{u}_h) \in \mathbf{H}_{\mathbf{0}} \times [H^1(\Omega)]^d$, using the ellipticity of the bilinear form $A(\cdot,\cdot)$, we deduce that

$$C_{\mathtt{ell}}\, \|(\boldsymbol{\sigma}_{\mathbf{0}} - \boldsymbol{\sigma}_{\mathbf{0},h}, \mathbf{u} - \mathbf{u}_h)\|_{\mathbf{H}_{\mathbf{0}}\times[H^1(\Omega)]^d} \,\leq\, \sup_{\substack{(\boldsymbol{\tau},\mathbf{v})\in\mathbf{H}_{\mathbf{0}}\times[H^1(\Omega)]^d \\ (\boldsymbol{\tau},\mathbf{v})\neq(\mathbf{0},\mathbf{0})}} \frac{R(\boldsymbol{\tau}, \mathbf{v})}{\|(\boldsymbol{\tau}, \mathbf{v})\|_{\mathbf{H}_{\mathbf{0}}\times[H^1(\Omega)]^d}}.$$

Therefore, in order to derive a residual-based a posteriori indicator for the total error, it is enough to bound the residual R in terms of computable local quantities.

Now, after some algebraic manipulations, we have that

$$R(\boldsymbol{\tau}, \mathbf{v}) = R_1(\boldsymbol{\tau}) + R_2(\mathbf{v}), \qquad \forall\, \boldsymbol{\tau} \in \mathbf{H}_{\mathbf{0}}, \quad \forall\, \mathbf{v} \in [H^1(\Omega)]^d, \tag{15}$$

where

$$\begin{aligned} R_1(\boldsymbol{\tau}) &:= \int_{\Omega} (\boldsymbol{\zeta} + \nabla \mathbf{u}_h - \frac{1}{\nu}\,\boldsymbol{\sigma}^{\mathtt{d}}_{\mathbf{0},h}) : \boldsymbol{\tau} + \langle \boldsymbol{\tau}\mathbf{n}, \mathbf{u}_D - \mathbf{u}_h\rangle_{\Gamma_D} \\ &- \kappa_1 \int_{\Omega} (\tilde{\mathbf{f}} + \mathbf{div}(\boldsymbol{\sigma}_{\mathbf{0},h}) - \mathbf{a}\cdot\nabla\mathbf{u}_h)\cdot\mathbf{div}(\boldsymbol{\tau}) - \frac{\kappa_2}{\nu}\int_{\Omega} (\boldsymbol{\zeta} + \nabla\mathbf{u}_h - \frac{1}{\nu}\,\boldsymbol{\sigma}^{\mathtt{d}}_{\mathbf{0},h}) : \boldsymbol{\tau}^{\mathtt{d}}, \end{aligned} \tag{16}$$

and

$$R_2(\mathbf{v}) := \int_\Omega (\tilde{\mathbf{f}} + \mathbf{div}(\boldsymbol{\sigma}_{\mathbf{0},h}) - \mathbf{a}\cdot\nabla\mathbf{u}_h)\cdot\mathbf{v} - \kappa_1 \int_\Omega (\tilde{\mathbf{f}} + \mathbf{div}(\boldsymbol{\sigma}_{\mathbf{0},h}) - \mathbf{a}\cdot\nabla\mathbf{u}_h)\cdot(\mathbf{a}\cdot\nabla\mathbf{v}) \\ - \kappa_2 \int_\Omega (\boldsymbol{\zeta} + \nabla\mathbf{u}_h - \frac{1}{\nu}\boldsymbol{\sigma}^{\mathrm{d}}_{\mathbf{0},h}) : \nabla\mathbf{v} + \kappa_3 \int_{\Gamma_D} (\mathbf{u}_D - \mathbf{u}_h)\cdot\mathbf{v}\,. \tag{17}$$

In the next subsections, we proceed to bound the residual components R_1 and R_2 in two and three dimensions, respectively. Before, we introduce some notations and recall some results concerning the Clément and Raviart–Thomas interpolation operators.

Given $T \in \mathcal{T}_h$, we let $E(T)$ be the set of its edges ($d = 2$) or faces ($d = 3$), and let $E_h := \cup_{T\in\mathcal{T}_h} E(T)$. Then, we can write $E_h = E_I \cup E_{\Gamma_D} \cup E_{\Gamma_N}$, where $E_I := \{e \in E_h : e \subseteq \Omega\}$, $E_{\Gamma_D} := \{e \in E_h : e \subseteq \Gamma_D\}$ and $E_{\Gamma_N} := \{e \in E_h : e \subseteq \Gamma_N\}$. Moreover, for each edge (resp., face) $e \in E_h$, we denote by h_e its diameter and fix a unit normal vector $\mathbf{n}_e := (n_1, n_2)^{\mathrm{t}}$ (resp., $\mathbf{n}_e := (n_1, n_2, n_3)^{\mathrm{t}}$). If $d = 2$, we let $\mathbf{t}_e := (-n_2, n_1)^{\mathrm{t}}$ be the corresponding fixed (unit) tangential vector along e. From now on, when no confusion arises, we simply write $\mathbf{n}$ and $\mathbf{t}$ instead of $\mathbf{n}_e$ and $\mathbf{t}_e$, respectively.

We will use the Clément interpolation operator $I_h : H^1(\Omega) \to \mathcal{L}_m$ (cf. [16]). The following Lemma establishes the local approximation properties of I_h.

Lemma 4. *There exist positive constants, c_3 and c_4, independent of h, such that for all $v \in H^1(\Omega)$ there holds*

$$\|v - I_h(v)\|_{H^l(T)} \le c_3\, h_T^{1-l} \|v\|_{H^1(\omega(T))}\,, \quad \forall\, l \in \{0,1\}\,, \quad \forall\, T \in \mathcal{T}_h,$$

and

$$\|v - I_h(v)\|_{L^2(e)} \le c_4\, h_e^{1/2} \|v\|_{H^1(\omega(e))}\,, \quad \forall\, e \in E_h,$$

where $\omega(T) := \cup\{T' \in \mathcal{T}_h : T' \cap T \neq \emptyset\}$ and $\omega(e) := \cup\{T' \in \mathcal{T}_h : T' \cap e \neq \emptyset\}$.

Proof. See Theorem 1 in [16]. □

We also consider the Raviart–Thomas interpolation operator, $\Pi_h^k : [H^1(\Omega)]^{d\times d} \to \mathbf{H}_{\mathbf{0},h}$ (cf. [13,15]), which, given $\boldsymbol{\tau} \in [H^1(\Omega)]^{d\times d}$, is characterized by the following identities:

$$\int_e \Pi_h^k(\boldsymbol{\tau})\mathbf{n}\cdot\mathbf{q} = \int_e \boldsymbol{\tau}\mathbf{n}\cdot\mathbf{q}\,, \quad \forall e \in E_h\,, \quad \forall\, \mathbf{q} \in [\mathcal{P}_k(e)]^d\,, \quad \text{when } k \ge 0\,, \tag{18}$$

and

$$\int_T \Pi_h^k(\boldsymbol{\tau}) : \boldsymbol{\rho} = \int_T \boldsymbol{\tau} : \boldsymbol{\rho}\,, \quad \forall\, T \in \mathcal{T}_h\,, \quad \forall\, \boldsymbol{\rho} \in [\mathcal{P}_{k-1}(T)]^{d\times d}\,, \quad \text{when } k \ge 1\,. \tag{19}$$

In the next Lemma, we recall the approximation properties of the operator Π_h^k.

Lemma 5. *There exists a positive constant c_5, independent of h, such that for all $T \in \mathcal{T}_h$*

$$\|\boldsymbol{\tau} - \Pi_h^k(\boldsymbol{\tau})\|_{[L^2(T)]^{d\times d}} \le c_5\, h_T^m\, |\boldsymbol{\tau}|_{[H^m(T)]^{d\times d}}\,, \quad \forall\, \boldsymbol{\tau} \in [H^m(\Omega)]^{d\times d} \quad 1 \le m \le k+1\,. \tag{20}$$

Moreover, there exist positive constants, c_6 and c_7, independent of h, such that for all $\boldsymbol{\tau} \in [H^{m+1}(\Omega)]^{d\times d}$ with $\mathbf{div}(\boldsymbol{\tau}) \in [H^m(\Omega)]^d$,

$$\|\mathbf{div}(\boldsymbol{\tau} - \Pi_h^k(\boldsymbol{\tau}))\|_{[L^2(T)]^d} \le c_6\, h_T^m\, |\mathbf{div}(\boldsymbol{\tau})|_{[H^m(T)]^d}\,, \quad 0 \le m \le k+1\,, \tag{21}$$

and

$$\|\boldsymbol{\tau}\mathbf{n} - \Pi_h^k(\boldsymbol{\tau})\mathbf{n}\|_{[L^2(e)]^d} \le c_7\, h_e^{1/2}\, \|\boldsymbol{\tau}\|_{[H^1(T_e)]^{d\times d}}\,, \quad \forall\, e \in E_h\,, \quad \forall\, \boldsymbol{\tau} \in [H^1(\Omega)]^{d\times d}\,, \tag{22}$$

where T_e is the triangle in $\mathcal{T}_h$ which contains e on its boundary.

Proof. See e.g. [13] or [15]. □

Using (18) and (19), one can show that (cf. [13,15])

$$\mathbf{div}(\Pi_h^k(\boldsymbol{\tau})) \,=\, P_h^k(\mathbf{div}(\boldsymbol{\tau}))\,, \tag{23}$$

where $P_h^k \,:\, [L^2(\Omega)]^d \,\to\, \mathbf{V}_h$ is the L^2-orthogonal projector. It is well known (see, e.g. [17]) that for each $\mathbf{v} \in [H^m(\Omega)]^d$, with $0 \leq m \leq k+1$, there holds

$$\|\mathbf{v} - P_h^k(\mathbf{v})\|_{[L^2(T)]^d} \,\leq\, C\, h_T^m\, |\mathbf{v}|_{[H^m(T)]^d}\,, \quad \forall\, T \in \mathcal{T}_h\,. \tag{24}$$

5.1. Two-dimensional a posteriori error analysis

In this subsection, we partially follow [11] and employ a quasi-Helmholtz decomposition of the $H(\mathbf{div};\Omega)$-variable (cf. [10]) to derive a residual-based a posteriori error indicator for the augmented mixed finite element methods (10) in the two-dimensional case. We first prove the reliability of the a posteriori error indicator and then, its local efficiency.

5.1.1. Reliability

We proceed to bound the residual components R_1 and R_2 when $d = 2$. Throughout this section, given a vector valued field $\mathbf{v} := (v_1, v_2)^{\mathtt{t}}$, we denote

$$\underline{\mathbf{curl}}(\mathbf{v}) := \begin{pmatrix} \frac{\partial v_1}{\partial x_2} & -\frac{\partial v_1}{\partial x_1} \\ \frac{\partial v_2}{\partial x_2} & -\frac{\partial v_2}{\partial x_1} \end{pmatrix}.$$

Let $\boldsymbol{\tau} \in \mathbf{H_0}$ be arbitrary and consider its quasi-Helmholtz decomposition (cf. Lemma 5.1 in [10]):

$$\boldsymbol{\tau} = \underline{\mathbf{curl}}(\boldsymbol{\chi}) \,+\, \boldsymbol{\Phi}\,, \tag{25}$$

where $\boldsymbol{\chi} \in [H^1(\Omega)]^2$ and $\boldsymbol{\Phi} \in [H^1(\Omega)]^{2\times 2}$ are such that $\underline{\mathbf{curl}}(\boldsymbol{\chi})\mathbf{n} = \mathbf{0}$ on Γ_N and $\boldsymbol{\Phi}\mathbf{n} = \mathbf{0}$ on Γ_N. Moreover, there exists $C > 0$, independent of h, such that

$$\|\boldsymbol{\chi}\|_{[H^1(\Omega)]^2} \,+\, \|\boldsymbol{\Phi}\|_{[H^1(\Omega)]^{2\times 2}} \,\leq\, C\, \|\boldsymbol{\tau}\|_{H(\mathbf{div};\Omega)}\,. \tag{26}$$

Clearly, $\mathbf{div}(\boldsymbol{\Phi}) = \mathbf{div}(\boldsymbol{\tau})$ in Ω.

Then, we let $\boldsymbol{\chi}_h := \mathbf{I}_h(\boldsymbol{\chi})$, where $\mathbf{I}_h \,:\, [H^1(\Omega)]^2 \to \mathbf{V}_h$ is defined componentwise by I_h, and define

$$\boldsymbol{\tau}_h := \underline{\mathbf{curl}}(\boldsymbol{\chi}_h) \,+\, \Pi_h^k(\boldsymbol{\Phi}) \in \mathbf{H}_{\mathbf{0},h}\,. \tag{27}$$

We refer to (27) as a *discrete quasi-Helmholtz decomposition* of $\boldsymbol{\tau}_h$.

Therefore, we can write

$$\boldsymbol{\tau} - \boldsymbol{\tau}_h \,=\, \underline{\mathbf{curl}}(\boldsymbol{\chi} - \boldsymbol{\chi}_h) \,+\, \boldsymbol{\Phi} - \Pi_h^k(\boldsymbol{\Phi})\,, \tag{28}$$

which, using (23) and that $\mathbf{div}(\boldsymbol{\Phi}) = \mathbf{div}(\boldsymbol{\tau})$ in Ω, yields

$$\mathbf{div}(\boldsymbol{\tau} - \boldsymbol{\tau}_h) \,=\, \mathbf{div}(\boldsymbol{\Phi} - \Pi_h^k(\boldsymbol{\Phi})) \,=\, (I - P_h^k)(\mathbf{div}(\boldsymbol{\Phi})) \,=\, (I - P_h^k)(\mathbf{div}(\boldsymbol{\tau}))\,. \tag{29}$$

Hence, taking into account (28) and (29), we can write

$$R_1(\boldsymbol{\tau}) \,=\, R_1(\boldsymbol{\tau} - \boldsymbol{\tau}_h) \,=\, \bar{R}_1(\boldsymbol{\tau}) \,+\, \hat{R}_1(\boldsymbol{\Phi}) \,+\, \tilde{R}_1(\boldsymbol{\chi})\,, \tag{30}$$

where

$$\bar{R}_1(\boldsymbol{\tau}) \,:=\, -\kappa_1 \int_\Omega (\tilde{\mathbf{f}} \,+\, \mathbf{div}(\boldsymbol{\sigma}_{\mathbf{0},h}) - \mathbf{a}\cdot\nabla\mathbf{u}_h)\cdot(I - P_h^k)(\mathbf{div}(\boldsymbol{\tau}))\,, \tag{31}$$

$$\begin{aligned} \hat{R}_1(\boldsymbol{\Phi}) \,:=\, \langle(\boldsymbol{\Phi} - \Pi_h^k(\boldsymbol{\Phi}))\mathbf{n}, \mathbf{u}_D - \mathbf{u}_h\rangle_{\Gamma_D} \,-\, \frac{\kappa_2}{\nu}\int_\Omega (\boldsymbol{\zeta} + \nabla\mathbf{u}_h - \frac{1}{\nu}\,\boldsymbol{\sigma}_{\mathbf{0},h}^{\mathtt{d}}) \,:\, (\boldsymbol{\Phi} - \Pi_h^k(\boldsymbol{\Phi}))^{\mathtt{d}} \\ +\, \int_\Omega (\boldsymbol{\zeta} + \nabla\mathbf{u}_h - \frac{1}{\nu}\,\boldsymbol{\sigma}_{\mathbf{0},h}^{\mathtt{d}}) \,:\, (\boldsymbol{\Phi} - \Pi_h^k(\boldsymbol{\Phi}))\,, \end{aligned} \tag{32}$$

and

$$\tilde{R}_1(\boldsymbol{\chi}) := \langle(\underline{\mathbf{curl}}(\boldsymbol{\chi}-\boldsymbol{\chi}_h))\mathbf{n}, \mathbf{u}_D-\mathbf{u}_h\rangle_{\Gamma_D} - \frac{\kappa_2}{\nu}\int_\Omega(\boldsymbol{\zeta}+\nabla\mathbf{u}_h-\frac{1}{\nu}\boldsymbol{\sigma}^{\mathtt{d}}_{\mathbf{0},h}) : (\underline{\mathbf{curl}}(\boldsymbol{\chi}-\boldsymbol{\chi}_h))^{\mathtt{d}} + \int_\Omega(\boldsymbol{\zeta}+\nabla\mathbf{u}_h-\frac{1}{\nu}\boldsymbol{\sigma}^{\mathtt{d}}_{\mathbf{0},h}) : \underline{\mathbf{curl}}(\boldsymbol{\chi}-\boldsymbol{\chi}_h)\,. \tag{33}$$

Our aim now is to obtain upper bounds for each one of the terms $\bar{R}_1(\boldsymbol{\tau})$, $\hat{R}_1(\boldsymbol{\Phi})$ and $\tilde{R}_1(\boldsymbol{\chi})$.

Lemma 6. *For any $\boldsymbol{\tau}\in H(\mathbf{div};\Omega)$, there holds*

$$|\bar{R}_1(\boldsymbol{\tau})| \le C\Big(\sum_{T\in\mathcal{T}_h}\kappa_1^2\,\|\tilde{\mathbf{f}}+\mathbf{div}(\boldsymbol{\sigma}_{\mathbf{0},h})-\mathbf{a}\cdot\nabla\mathbf{u}_h\|^2_{[L^2(T)]^2}\Big)^{1/2}\|\mathbf{div}(\boldsymbol{\tau})\|_{[L^2(\Omega)]^2},$$

where C is the constant in (24).

Proof. The proof follows by applying the Cauchy–Schwarz inequality in each element $T\in\mathcal{T}_h$ and inequality (24). □

Lemma 7. *There exists $C>0$, independent of h, ν and $\mathbf{a}$, such that*

$$|\hat{R}_1(\boldsymbol{\Phi})| \le C\Big(\sum_{e\in E_{\Gamma_D}} h_e\,\|\mathbf{u}_D-\mathbf{u}_h\|^2_{[L^2(e)]^2} + \sum_{T\in\mathcal{T}_h}h_T^2\Big(1+\frac{\kappa_2}{\nu}\Big)^2\|\boldsymbol{\zeta}+\nabla\mathbf{u}_h-\frac{1}{\nu}\boldsymbol{\sigma}^{\mathtt{d}}_{\mathbf{0},h}\|^2_{[L^2(T)]^{2\times2}}\Big)^{1/2}\|\boldsymbol{\tau}\|_{H(\mathbf{div};\Omega)}\,.$$

Proof. Since $\boldsymbol{\Phi}\in[H^1(\Omega)]^{2\times2}$, using the Cauchy–Schwarz inequality and (22), we have

$$|\langle(\boldsymbol{\Phi}-\Pi_h^k(\boldsymbol{\Phi}))\mathbf{n}, \mathbf{u}_D-\mathbf{u}_h\rangle_{\Gamma_D}| \le \sum_{e\in E_{\Gamma_D}}\Big|\int_e(\mathbf{u}_D-\mathbf{u}_h)\cdot(\boldsymbol{\Phi}-\Pi_h^k(\boldsymbol{\Phi}))\mathbf{n}\Big|$$

$$\le \sum_{e\in E_{\Gamma_D}}\|(\boldsymbol{\Phi}-\Pi_h^k(\boldsymbol{\Phi}))\mathbf{n}\|_{[L^2(e)]^2}\|\mathbf{u}_D-\mathbf{u}_h\|_{[L^2(e)]^2} \le c_7\sum_{e\in E_{\Gamma_D}}h_e^{1/2}\|\boldsymbol{\Phi}\|_{[H^1(T_e)]^{2\times2}}\|\mathbf{u}_D-\mathbf{u}_h\|_{[L^2(e)]^2}$$

$$\le c_7\Big(\sum_{e\in E_{\Gamma_D}}h_e\|\mathbf{u}_D-\mathbf{u}_h\|^2_{[L^2(e)]^2}\Big)^{1/2}\Big(\sum_{e\in E_{\Gamma_D}}\|\boldsymbol{\Phi}\|^2_{[H^1(T_e)]^{2\times2}}\Big)^{1/2}$$

$$\le c_7\Big(\sum_{e\in E_{\Gamma_D}}h_e\|\mathbf{u}_D-\mathbf{u}_h\|^2_{[L^2(e)]^2}\Big)^{1/2}\|\boldsymbol{\Phi}\|_{[H^1(\Omega)]^{2\times2}}\,.$$

Now, since $\|\boldsymbol{\Phi}\|_{[H^1(\Omega)]^{2\times2}}\le C\,\|\boldsymbol{\tau}\|_{H(\mathbf{div};\Omega)}$ (see (26)), we deduce

$$|\langle(\boldsymbol{\Phi}-\Pi_h^k(\boldsymbol{\Phi}))\mathbf{n}, \mathbf{u}_D-\mathbf{u}_h\rangle_{\Gamma_D}| \le C\Big(\sum_{e\in E_{\Gamma_D}}h_e\,\|\mathbf{u}_D-\mathbf{u}_h\|^2_{[L^2(e)]^2}\Big)^{1/2}\|\boldsymbol{\tau}\|_{H(\mathbf{div};\Omega)}\,.$$

Similarly, using (20) with $m=1$, we obtain

$$\Big|\int_\Omega(\boldsymbol{\zeta}+\nabla\mathbf{u}_h-\frac{1}{\nu}\boldsymbol{\sigma}^{\mathtt{d}}_{\mathbf{0},h}) : (\boldsymbol{\Phi}-\Pi_h^k(\boldsymbol{\Phi}))\Big| \le C\Big(\sum_{T\in\mathcal{T}_h}h_T^2\,\|\boldsymbol{\zeta}+\nabla\mathbf{u}_h-\frac{1}{\nu}\boldsymbol{\sigma}^{\mathtt{d}}_{\mathbf{0},h}\|^2_{[L^2(T)]^{2\times2}}\Big)^{1/2}\|\boldsymbol{\tau}\|_{H(\mathbf{div};\Omega)}.$$

Therefore, the proof is complete by using the triangle inequality and that $\|\boldsymbol{\tau}^{\mathtt{d}}\|_{[L^2(T)]^{2\times2}}\le\|\boldsymbol{\tau}\|_{[L^2(T)]^{2\times2}}$. □

Lemma 8. *Assume* $\mathbf{u}_D \in [H^1(\Gamma_D)]^2$. *Then, there exists* $C > 0$, *independent of* h, ν *and* $\mathbf{a}$ *such that*

$$|\tilde{R}_1(\boldsymbol{\chi})| \leq C \Big(\sum_{T\in\mathcal{T}_h} \Big(1+\frac{\kappa_2}{\nu}\Big)^2 \|\boldsymbol{\zeta} + \nabla \mathbf{u}_h - \frac{1}{\nu}\boldsymbol{\sigma}^{\mathrm{d}}_{\mathbf{0},h}\|^2_{[L^2(T)]^{2\times 2}} + \sum_{e\in E_{\Gamma_D}} h_e \left\| \frac{d\mathbf{u}_D}{d\mathbf{t}} - \frac{d\mathbf{u}_h}{d\mathbf{t}} \right\|^2_{[L^2(e)]^2} \Big)^{1/2} \|\boldsymbol{\tau}\|_{H(\mathbf{div};\Omega)} .$$

Proof. We first remark that, for each $T \in \mathcal{T}_h$ we have

$$\|\underline{\mathbf{curl}}(\boldsymbol{\chi} - \boldsymbol{\chi}_h)\|_{[L^2(T)]^{2\times 2}} = \|\nabla(\boldsymbol{\chi} - \boldsymbol{\chi}_h)\|_{[L^2(T)]^{2\times 2}} \leq \|\boldsymbol{\chi} - \boldsymbol{\chi}_h\|_{[H^1(T)]^2} ,$$

which, using Lemma 4, implies

$$\|\underline{\mathbf{curl}}(\boldsymbol{\chi} - \boldsymbol{\chi}_h)\|_{[L^2(T)]^{2\times 2}} \leq c_3 \|\boldsymbol{\chi}\|_{[H^1(\omega(T))]^2}.$$

Then, applying the Cauchy–Schwarz inequality, using that the number of triangles in $\omega(T)$ is bounded and that $\|\boldsymbol{\chi}\|_{[H^1(\Omega)]^2} \leq C \|\boldsymbol{\tau}\|_{H(\mathbf{div};\Omega)}$ (see (26)), we deduce

$$\left| \int_\Omega (\boldsymbol{\zeta} + \nabla \mathbf{u}_h - \frac{1}{\nu}\boldsymbol{\sigma}^{\mathrm{d}}_{\mathbf{0},h}) : \underline{\mathbf{curl}}(\boldsymbol{\chi} - \boldsymbol{\chi}_h) \right| \leq C \left(\sum_{T\in\mathcal{T}_h} \|\boldsymbol{\zeta} + \nabla \mathbf{u}_h - \frac{1}{\nu}\boldsymbol{\sigma}^{\mathrm{d}}_{\mathbf{0},h}\|^2_{[L^2(T)]^{2\times 2}} \right)^{1/2} \|\boldsymbol{\tau}\|_{H(\mathbf{div};\Omega)} .$$

On the other hand, using that $\underline{\mathbf{curl}}(\boldsymbol{\chi} - \boldsymbol{\chi}_h)\mathbf{n} = -\frac{d}{d\mathbf{t}}(\boldsymbol{\chi} - \boldsymbol{\chi}_h)$ on Γ, we arrive

$$\langle (\underline{\mathbf{curl}}(\boldsymbol{\chi} - \boldsymbol{\chi}_h))\mathbf{n}, \mathbf{u}_D - \mathbf{u}_h\rangle_{\Gamma_D} = \langle \boldsymbol{\chi} - \boldsymbol{\chi}_h, \frac{d}{d\mathbf{t}}(\mathbf{u}_D - \mathbf{u}_h)\rangle_\Gamma,$$

so, thanks to Lemma 4, the proof follows similarly to the previous lemmas. □

On the other hand, we have the following bound for the residual R_2.

Lemma 9. *There exists a positive constant* C, *that depends on the constants* c_3 *and* c_4 *of Lemma 4, such that*

$$\begin{aligned} |R_2(\mathbf{v})| \quad &\leq \quad C \Big(\kappa_3^2 \sum_{e\in E_{\Gamma_D}} h_e \|\mathbf{u}_D - \mathbf{u}_h\|^2_{[L^2(e)]^2} + \sum_{T\in\mathcal{T}_h} \kappa_2^2 \|\boldsymbol{\zeta} + \nabla \mathbf{u}_h - \frac{1}{\nu}\boldsymbol{\sigma}^{\mathrm{d}}_{\mathbf{0},h}\|^2_{[L^2(T)]^2} \\ &+ \quad (h_T + \kappa_1\sqrt{2}\|\mathbf{a}\|_{[L^\infty(T)]^2})^2 \|\tilde{\mathbf{f}} + \mathbf{div}(\boldsymbol{\sigma}_{\mathbf{0},h}) - \mathbf{a}\cdot\nabla\mathbf{u}_h\|^2_{[L^2(T)]^2} \Big)^{1/2}. \end{aligned} \tag{34}$$

Proof. Using the orthogonality property, we deduce that $R_2(\mathbf{v}) = R_2(\mathbf{v} - \mathbf{I}_h(\mathbf{v}))$. Then, inequality (34) is achieved after applying the Cauchy–Schwarz inequality and Lemma 4. □

Now, motivated by the previous results, we define the global a posteriori error indicator $\eta := \left(\sum_{T\in\mathcal{T}_h} \eta_T^2\right)^{1/2}$, where the local error indicator η_T is given by

$$\begin{aligned} \eta_T^2 := \alpha_{1,T} \|\tilde{\mathbf{f}} + \mathbf{div}(\boldsymbol{\sigma}_{\mathbf{0},h}) - \mathbf{a}\cdot\nabla\mathbf{u}_h\|^2_{[L^2(T)]^2} + \alpha_{2,T} \|\boldsymbol{\zeta} + \nabla\mathbf{u}_h - \frac{1}{\nu}\boldsymbol{\sigma}^{\mathrm{d}}_{\mathbf{0},h}\|^2_{[L^2(T)]^{2\times 2}} \\ + \sum_{e\in E_{\Gamma_D}\cap\partial T} h_e \left(\alpha_{3,T} \|\mathbf{u}_D - \mathbf{u}_h\|^2_{[L^2(e)]^2} + \left\| \frac{d\mathbf{u}_D}{d\mathbf{t}} - \frac{d\mathbf{u}_h}{d\mathbf{t}} \right\|^2_{[L^2(e)]^2} \right). \end{aligned} \tag{35}$$

with

$$\alpha_{1,T} := \kappa_1^2 + (h_T + \kappa_1\sqrt{2}\|\mathbf{a}\|_{[L^\infty(T)]^2})^2 , \qquad \alpha_{2,T} := \kappa_2^2 + (1+h_T^2)\left(1+\frac{\kappa_2}{\nu}\right)^2 , \qquad \alpha_{3,T} := 1 + \kappa_3^2.$$

We remark that, if we define $\boldsymbol{\sigma}_h := \boldsymbol{\sigma}_{\mathbf{0},h} + \boldsymbol{\sigma}_{\mathbf{g}}$, using the definitions of $\tilde{\mathbf{f}}$ and $\boldsymbol{\zeta}$, the first two residual terms can be rewritten as follows:

$$\|\tilde{\mathbf{f}} + \mathbf{div}(\boldsymbol{\sigma}_{\mathbf{0},h}) - \mathbf{a}\cdot\nabla\mathbf{u}_h\|_{[L^2(T)]^2} = \|\mathbf{f} + \mathbf{div}(\boldsymbol{\sigma}_h) - \mathbf{a}\cdot\nabla\mathbf{u}_h\|_{[L^2(T)]^2}$$

and

$$\|\boldsymbol{\zeta} + \nabla \mathbf{u}_h - \frac{1}{\nu}\boldsymbol{\sigma}^{\mathrm{d}}_{\mathbf{0},h}\|_{[L^2(T)]^{2\times 2}} = \|\nabla \mathbf{u}_h - \frac{1}{\nu}\boldsymbol{\sigma}^{\mathrm{d}}_{h}\|_{[L^2(T)]^{2\times 2}}.$$

Let us notice that, since we assumed that $\mathbf{g}$ is componentwise a piecewise polynomial of degree at most k over the initial mesh, then $\boldsymbol{\sigma}_h$ is in the corresponding Raviart–Thomas space.

Finally, we use the previous lemmas to obtain the following Theorem, which establishes the reliability of the a posteriori error indicator η.

Theorem 4. *Assume $\mathbf{u}_D \in [H^1(\Gamma_D)]^2$. Then, there exists $C > 0$, independent of h, ν and $\mathbf{a}$, such that*

$$\|(\boldsymbol{\sigma}_{\mathbf{0}} - \boldsymbol{\sigma}_{\mathbf{0},h}, \mathbf{u} - \mathbf{u}_h)\|_{\mathbf{H}_0 \times [H^1(\Omega)]^2} \leq C\, C_{\mathtt{ell}}^{-1}\, \eta\,. \tag{36}$$

Proof. It follows from (14), (15), (25), (30), the triangle inequality, (26) and Lemmas 6, 7, 8 and 9. □

In the next subsection we establish the local efficiency of the a posteriori error indicator η.

5.1.2. Local efficiency

We first remark that, since $\tilde{\mathbf{f}} = -\mathbf{div}(\boldsymbol{\sigma}_{\mathbf{0}}) + \mathbf{a}\cdot\nabla\mathbf{u}$ in Ω and $\boldsymbol{\zeta} = \frac{1}{\nu}\boldsymbol{\sigma}^{\mathrm{d}}_{\mathbf{0}} - \nabla\mathbf{u}$ in Ω, we have that

$$\|\tilde{\mathbf{f}} + \mathbf{div}(\boldsymbol{\sigma}_{\mathbf{0},h}) - \mathbf{a}\cdot\nabla\mathbf{u}_h\|_{[L^2(T)]^2} \leq \sqrt{2}\,\|\mathbf{a}\|_{[L^\infty(T)]^2}\,\|\nabla(\mathbf{u}-\mathbf{u}_h)\|_{[L^2(T)]^{2\times 2}} + \|\mathbf{div}(\boldsymbol{\sigma}_{\mathbf{0}} - \boldsymbol{\sigma}_{\mathbf{0},h})\|_{[L^2(T)]^2}\,, \tag{37}$$

and

$$\|\boldsymbol{\zeta} + \nabla\mathbf{u}_h - \frac{1}{\nu}\boldsymbol{\sigma}^{\mathrm{d}}_{\mathbf{0},h}\|_{[L^2(T)]^{2\times 2}} \leq |\mathbf{u}-\mathbf{u}_h|_{[H^1(T)]^2} + \frac{1}{\nu}\,\|\boldsymbol{\sigma}_{\mathbf{0}} - \boldsymbol{\sigma}_{\mathbf{0},h}\|_{[L^2(T)]^{2\times 2}}\,. \tag{38}$$

Now, in order to bound the boundary residual terms, we proceed similarly as in [11].

Lemma 10. *There exists $c_8 > 0$, independent of h, such that for each $e \in E_{\Gamma_D}$, there holds*

$$h_e\|\mathbf{u}_D - \mathbf{u}_h\|^2_{[L^2(e)]^2} \leq c_8\left(\|\mathbf{u}-\mathbf{u}_h\|^2_{[L^2(T_e)]^2} + h^2_{T_e}|\mathbf{u}-\mathbf{u}_h|^2_{[H^1(T_e)]^2}\right),$$

where T_e is the triangle in $\mathcal{T}_h$ having e as an edge.

Proof. There exists $c > 0$, depending only on the shape regularity of the triangulations, such that for each $T \in \mathcal{T}_h$ and $e \in E(T)$, the following discrete trace inequality holds (cf. Theorem 3.10 in [18]):

$$\|v\|^2_{L^2(e)} \leq c\left\{h_e^{-1}\,\|v\|^2_{L^2(T)} + h_e\,|v|^2_{H^1(T)}\right\}, \quad \forall\, v \in H^1(T)\,. \tag{39}$$

The result is a straightforward application of (39), taking into account that $\mathbf{u} = \mathbf{u}_D$ on Γ_D. □

Lemma 11. *Assume $\mathbf{u}_D \in [H^1(\Gamma_D)]^2$ is component-wise a piecewise polynomial on Γ_D. Then there exists $c_9 > 0$, independent of h, such that for each $e \in E_{\Gamma_D}$ there holds*

$$h_e\left\|\frac{d\mathbf{u}_D}{d\mathbf{t}} - \frac{d\mathbf{u}_h}{d\mathbf{t}}\right\|^2_{[L^2(e)]^2} \leq c_9\,|\mathbf{u}-\mathbf{u}_h|^2_{[H^1(T_e)]^2}\,, \tag{40}$$

where T_e is the triangle having e as an edge.

Proof. See Lemma 3.10 in [11]. □

In summary we have proved the next Theorem, which establishes the local efficiency of the a posteriori error indicator η.

Theorem 5. *Assume $\mathbf{u}_D \in [H^1(\Gamma_D)]^2$ is component-wise a piecewise polynomial on Γ_D. Then, there exists a positive constant $C_{\mathtt{eff}}$, independent of h, such that for all $T \in \mathcal{T}_h$ we have*

$$\eta^2_T \leq C_{\mathtt{eff}}\left(\|\mathbf{u}-\mathbf{u}_h\|^2_{[H^1(T)]^2} + \|\boldsymbol{\sigma}_{\mathbf{0}} - \boldsymbol{\sigma}_{\mathbf{0},h}\|^2_{H(\mathbf{div},T)}\right).$$

Proof. It follows from the definition of η_T, applying (37), (38) and Lemmas 10 and 11. □

5.2. Three-dimensional a posteriori error analysis

In the three-dimensional case, if the domain Ω is non-convex, the a posteriori error analysis is restricted to the situation where Γ_N is connected and can be contained in the boundary of a convex extension of Ω (see Theorem 3.2 in [12]). So, we assume that there exists a convex three-dimensional domain Σ such that

$$\Omega \subset \Sigma\,, \quad \text{and} \quad \Gamma_N \subset \partial\Sigma.$$

In this situation, given $\boldsymbol{\tau} \in \mathbf{H}_0$, there exist $\mathbf{z} \in [H^2(\Omega)]^3$ and $\boldsymbol{\chi} \in [H^1(\Omega)]^{3\times 3}$, with $\boldsymbol{\chi} = \mathbf{0}$ on Γ_N, such that

$$\boldsymbol{\tau} = \nabla \mathbf{z} + \underline{\mathbf{curl}}\,\boldsymbol{\chi}\,, \tag{41}$$

with

$$\underline{\mathbf{curl}}(\boldsymbol{\chi}) := \begin{pmatrix} \mathbf{curl}(\chi_{11}, \chi_{12}, \chi_{13}) \\ \mathbf{curl}(\chi_{21}, \chi_{22}, \chi_{23}) \\ \mathbf{curl}(\chi_{31}, \chi_{32}, \chi_{33}) \end{pmatrix},$$

and there exists a positive constant C such that

$$\|\mathbf{z}\|_{[H^2(\Omega)]^3} + \|\boldsymbol{\chi}\|_{[H^1(\Omega)]^{3\times 3}} \leq C \|\boldsymbol{\tau}\|_{H(\mathbf{div},\Omega)}\,. \tag{42}$$

Then, we define $\boldsymbol{\chi}_h = \mathbf{I}_h(\boldsymbol{\chi})$, with $\mathbf{I}_h$ defined componentwise by I_h, and

$$\boldsymbol{\tau}_h = \Pi_h^k \nabla \mathbf{z} + \underline{\mathbf{curl}}\,\boldsymbol{\chi}_h.$$

Therefore, we have that

$$\boldsymbol{\tau} - \boldsymbol{\tau}_h = (I - \Pi_h^k)\nabla \mathbf{z} + \underline{\mathbf{curl}}(\boldsymbol{\chi} - \boldsymbol{\chi}_h)$$

and

$$\mathrm{div}(\boldsymbol{\tau} - \boldsymbol{\tau}_h) = (I - P_k^k)\Delta \mathbf{z} = (I - P_k^k)\mathbf{div}(\boldsymbol{\tau}).$$

So, we have the analogue of (30):

$$R_1(\boldsymbol{\tau}) \;=\; \bar{R}_1(\boldsymbol{\tau}) \;+\; \hat{R}_1(\mathbf{z}) \;+\; \tilde{R}_1(\boldsymbol{\chi})\,, \tag{43}$$

with $\bar{R}_1(\boldsymbol{\tau})$ and $\tilde{R}_1(\boldsymbol{\chi})$ formally defined as in (31) and (33), respectively, and

$$\begin{aligned} \hat{R}_1(\mathbf{z}) \;:=\; \langle (I - \Pi_h^k)\nabla \mathbf{z} \cdot \mathbf{n}, \mathbf{u}_D - \mathbf{u}_h \rangle_{\Gamma_D} \;-\; \frac{\kappa_2}{\nu} \int_\Omega (\boldsymbol{\zeta} + \nabla \mathbf{u}_h - \frac{1}{\nu}\,\boldsymbol{\sigma}^{\mathrm{d}}_{\mathbf{0},h}) \,:\, ((I - \Pi_h^k)\nabla \mathbf{z})^{\mathrm{d}} \\ + \int_\Omega (\boldsymbol{\zeta} + \nabla \mathbf{u}_h - \frac{1}{\nu}\,\boldsymbol{\sigma}^{\mathrm{d}}_{\mathbf{0},h}) \,:\, (I - \Pi_h^k)\nabla \mathbf{z}\,. \end{aligned} \tag{44}$$

The first term on the right-hand side of (43) can be bounded exactly as in Lemma 6. The second term on the right-hand side of (43) can be bounded analogously to Lemma 7 by substituting formally $\boldsymbol{\Phi}$ by $\nabla \mathbf{z} \in [H^1(\Omega)]^{3\times 3}$ and using (42). Finally, from the definition of $\underline{\mathbf{curl}}(\boldsymbol{\chi} - \boldsymbol{\chi}_h)$, we have that

$$\langle \underline{\mathbf{curl}}(\boldsymbol{\chi} - \boldsymbol{\chi}_h)\mathbf{n}, \mathbf{u}_D - \mathbf{u}_h \rangle_{\Gamma_D} \;=\; \langle \boldsymbol{\chi} - \boldsymbol{\chi}_h, \nabla(\mathbf{u}_D - \mathbf{u}_h) \times \mathbf{n} \rangle_{\Gamma_D},$$

where we denote by $\nabla \mathbf{v} \times \mathbf{n}$ the vector product of each row of $\nabla \mathbf{v}$ by $\mathbf{n}$:

$$\nabla \mathbf{v} \times \mathbf{n} = \begin{pmatrix} \dfrac{\partial v_1}{\partial x_2} n_3 - \dfrac{\partial u_1}{\partial x_3} n_2 & \dfrac{\partial v_1}{\partial x_3} n_1 - \dfrac{\partial u_1}{\partial x_1} n_3 & \dfrac{\partial v_1}{\partial x_1} n_2 - \dfrac{\partial u_1}{\partial x_3} n_1 \\ \dfrac{\partial v_2}{\partial x_2} n_3 - \dfrac{\partial u_2}{\partial x_3} n_2 & \dfrac{\partial v_2}{\partial x_3} n_1 - \dfrac{\partial u_2}{\partial x_1} n_3 & \dfrac{\partial v_2}{\partial x_1} n_2 - \dfrac{\partial u_2}{\partial x_3} n_1 \\ \dfrac{\partial v_3}{\partial x_2} n_3 - \dfrac{\partial u_3}{\partial x_3} n_2 & \dfrac{\partial v_3}{\partial x_3} n_1 - \dfrac{\partial u_3}{\partial x_1} n_3 & \dfrac{\partial v_3}{\partial x_1} n_2 - \dfrac{\partial u_3}{\partial x_3} n_1 \end{pmatrix}.$$

Then, applying the Cauchy–Schwarz inequality and Lemma 4, we obtain that

$$|\langle \underline{\mathbf{curl}}(\boldsymbol{\chi} - \boldsymbol{\chi}_h)\mathbf{n}, \mathbf{u}_D - \mathbf{u}_h \rangle_{\Gamma_D}| \;\leq\; C\, c_4 \Big(\sum_{e \in E_{\Gamma_D}} h_e \|\nabla(\mathbf{u}_D - \mathbf{u}_h) \times \mathbf{n}\|^2_{[L^2(e)]^{3\times 3}} \Big)^{1/2} \|\boldsymbol{\tau}\|_{H(\mathbf{div},\Omega)}.$$

The second and third terms in the definition of $\tilde{R}_1(\boldsymbol{\chi})$ are bounded as in Lemma 8.

On the other hand, proceeding as in Lemma 9, we arrive at

$$\begin{aligned} |R_2(\mathbf{v})| \;\leq\; & C\,\Big(\kappa_3^2 \sum_{e\in E_{\Gamma_D}} h_e \|\mathbf{u}_D-\mathbf{u}_h\|^2_{[L^2(e)]^3} \;+\; \sum_{T\in\mathcal{T}_h} \kappa_2^2\, \|\boldsymbol{\zeta}+\nabla\mathbf{u}_h-\frac{1}{\nu}\,\boldsymbol{\sigma}^{\mathtt{d}}_{\mathbf{0},h}\|^2_{[L^2(T)]^3} \\ & +\; (h_T+\kappa_1\sqrt{3}\|\mathbf{a}\|_{[L^\infty(T)]^3})^2 \|\tilde{\mathbf{f}}+\mathbf{div}(\boldsymbol{\sigma}_{\mathbf{0},h})-\mathbf{a}\cdot\nabla\mathbf{u}_h\|^2_{[L^2(T)]^3}\Big)^{1/2}. \end{aligned} \tag{45}$$

Then, we propose the following a posteriori error indicator:

$$\begin{aligned} \tilde{\eta}_T^2 := \; & \tilde{\alpha}_{1,T}\|\tilde{\mathbf{f}}+\mathbf{div}(\boldsymbol{\sigma}_{\mathbf{0},h})-\mathbf{a}\cdot\nabla\mathbf{u}_h\|^2_{[L^2(T)]^3} \;+\; \tilde{\alpha}_{2,T}\|\boldsymbol{\zeta}+\nabla\mathbf{u}_h-\frac{1}{\nu}\,\boldsymbol{\sigma}^{\mathtt{d}}_{\mathbf{0},h}\|^2_{[L^2(T)]^3\times 3} \\ & +\sum_{e\in E_{\Gamma_D}\cap\partial T} h_e\left(\tilde{\alpha}_{3,T}\,\|\mathbf{u}_D-\mathbf{u}_h\|^2_{[L^2(e)]^3} \;+\; \|\nabla(\mathbf{u}_D-\mathbf{u}_h)\times\mathbf{n}\|^2_{[L^2(e)]^{3\times 3}}\right). \end{aligned} \tag{46}$$

with

$$\tilde{\alpha}_{1,T} := \kappa_1^2+(h_T+\kappa_1\sqrt{3}\|\mathbf{a}\|_{[L^\infty(T)]^3})^2\,, \qquad \tilde{\alpha}_{2,T} := \kappa_2^2+(1+h_T^2)\left(1+\frac{\kappa_2}{\nu}\right)^2\,, \qquad \tilde{\alpha}_{3,T} := 1+\kappa_3^2.$$

From the previous considerations, we have the following result, which establishes the reliability of the global a posteriori error indicator

$$\tilde{\eta} := \Big(\sum_{T\in\mathcal{T}_h}\tilde{\eta}_T^2\Big)^{1/2}. \tag{47}$$

Theorem 6. *Assume $\mathbf{u}_D\in[H^1(\Gamma_D)]^3$. Then, there exists $C>0$, independent of h, ν and $\mathbf{a}$, such that*

$$\|(\boldsymbol{\sigma}_{\mathbf{0}}-\boldsymbol{\sigma}_{\mathbf{0},h},\mathbf{u}-\mathbf{u}_h)\|_{\mathbf{H}_0\times[H^1(\Omega)]^3} \;\leq\; C\,C^{-1}_{\mathtt{ell}}\,\tilde{\eta}\,. \tag{48}$$

In order to prove the local efficiency of the a posteriori error indicator $\tilde{\eta}_T$, we proceed as in Section 5.1.2. More precisely, for the two first terms we have that

$$\|\tilde{\mathbf{f}}+\mathbf{div}(\boldsymbol{\sigma}_{0,h})-\mathbf{a}\cdot\nabla\mathbf{u}_h\|_{[L^2(T)]^3} \;\leq\; \sqrt{3}\,\|\mathbf{a}\|_{[L^\infty(T)]^3}\,\|\nabla(\mathbf{u}-\mathbf{u}_h)\|_{[L^2(T)]^{3\times 3}} \;+\; \|\mathbf{div}(\boldsymbol{\sigma}_0-\boldsymbol{\sigma}_{0,h})\|_{[L^2(T)]^3} \tag{49}$$

and

$$\|\boldsymbol{\zeta}+\nabla\mathbf{u}_h-\frac{1}{\nu}\,\boldsymbol{\sigma}^{\mathtt{d}}_{\mathbf{0},h}\|^2_{[L^2(T)]^{3\times 3}} \;\leq\; \|\nabla(\mathbf{u}-\mathbf{u}_h)\|_{[L^2(T)]^{3\times 3}} \;+\; \frac{1}{\nu}\|\boldsymbol{\sigma}_0-\boldsymbol{\sigma}_{0,h}\|_{[L^2(T)]^{3\times 3}}\,. \tag{50}$$

On the other hand, applying the discrete trace inequality (39) componentwise and using that $\mathbf{u}=\mathbf{u}_D$ on Γ_D, we obtain that for each $e\in E_{\Gamma_D}$, there holds

$$h_e\|\mathbf{u}_D-\mathbf{u}_h\|^2_{[L^2(e)]^3} \;\leq\; \tilde{c}_8\left(\|\mathbf{u}-\mathbf{u}_h\|^2_{[L^2(T_e)]^3} \;+\; h_{T_e}^2|\mathbf{u}-\mathbf{u}_h|^2_{[H^1(T_e)]^3}\right), \tag{51}$$

where T_e is the tetrahedra in $\mathcal{T}_h$ having e as a face and $\tilde{c}_8>0$ only depends on the shape regularity of the mesh.

Finally, we have the following result concerning the last boundary term:

Lemma 12. *Assume $\mathbf{u}_D\in[H^1(\Gamma_D)]^3$ is component-wise a piecewise polynomial on Γ_D. Then there exists $\tilde{c}_9>0$, independent of h, such that for each $e\in E_{\Gamma_D}$ there holds*

$$h_e\,\|\nabla(\mathbf{u}_D-\mathbf{u}_h)\times\mathbf{n}\|^2_{[L^2(e)]^{3\times 3}} \;\leq\; \tilde{c}_9\,|\mathbf{u}-\mathbf{u}_h|^2_{[H^1(T_e)]^3}\,, \tag{52}$$

where T_e is the tetrahedron having e as a face.

Proof. Let $e\in E_{\Gamma_D}$ and denote by $\boldsymbol{\chi}_e := \nabla(\mathbf{u}_D-\mathbf{u}_h)\times\mathbf{n}$ on e. We remark that $\boldsymbol{\chi}_e$ is a polynomial on e. Then, introducing the bubble function ψ_e (see [19]), we have that

$$\|\boldsymbol{\chi}_e\|^2_{[L^2(e)]^{3\times 3}} \;\leq\; c\,\|\psi_e^{1/2}\boldsymbol{\chi}_e\|^2_{[L^2(e)]^{3\times 3}} \;=\; c\int_e \psi_e\boldsymbol{\chi}_e : (\nabla(\mathbf{u}_D-\mathbf{u}_h)\times\mathbf{n}) \;=\; c\int_{\partial T_e}\psi_e\mathbf{L}(\boldsymbol{\chi}_e) : (\nabla(\mathbf{u}_D-\mathbf{u}_h)\times\mathbf{n})$$

where T_e is the tetrahedron having e as a face and $\mathbf{L}$ is an extension operator acting componentwise (see [19]).

Integrating by parts, using the Cauchy–Scwharz inequality and the properties of the extension operator $\mathbf{L}$ and the bubble function ψ_e (see [19]), we have that

$$\begin{aligned}\|\boldsymbol{\chi}_e\|^2_{[L^2(e)]^{3\times 3}} &\leq c\left|\int_{T_e}\underline{\mathbf{curl}}(\psi_e\mathbf{L}(\boldsymbol{\chi}_e)) : \nabla(\mathbf{u}-\mathbf{u}_h)\right| \\ &\leq C\,|\psi_e\mathbf{L}(\boldsymbol{\chi}_e)|_{[H^1(T_e)]^{3\times 3}}\,|\mathbf{u}-\mathbf{u}_h|_{[H^1(T_e)]^3} \\ &\leq C\,h_e^{1/2}\|\boldsymbol{\chi}_e\|_{[L^2(T_e)]^{3\times 3}}\,|\mathbf{u}-\mathbf{u}_h|_{[H^1(T_e)]^3}\end{aligned}$$

and the proof follows. □

In summary we have proved the next Theorem, which establishes the local efficiency of the a posteriori error indicator $\tilde{\eta}$.

Theorem 7. *Assume $\mathbf{u}_D \in [H^1(\Gamma_D)]^2$ is component-wise a piecewise polynomial on Γ_D. Then, there exists a positive constant $C_{\mathtt{eff}}$, independent of h, such that for all $T \in \mathcal{T}_h$ we have*

$$\tilde{\eta}_T^2 \leq C_{\mathtt{eff}}\left(\|\mathbf{u}-\mathbf{u}_h\|^2_{[H^1(T)]^3} + \|\boldsymbol{\sigma}_{\mathbf{0}}-\boldsymbol{\sigma}_{\mathbf{0},h}\|^2_{H(\mathbf{div},T)}\right).$$

Proof. It follows from the definition of $\tilde{\eta}_T$, applying (49), (50), (51) and Lemma 12. □

6. Numerical experiments

In this section, we present some numerical experiments that illustrate the performance of the augmented scheme (10) and confirm the properties of the a posteriori error indicators η and $\tilde{\eta}$ defined in (35) and (47), respectively.

The numerical experiments were performed with the finite element toolbox ALBERTA [20] using refinement by recursive bisection. The solution of the corresponding linear system is computed using the backslash operator of MATLAB. We present numerical experiments for the finite element pair $\left([\mathcal{RT}_0^+]^d, [\mathcal{L}_1]^d\right)$, for $d = 2$ and 3.

We use the standard adaptive finite element method (AFEM) based on the loop:

SOLVE → ESTIMATE → MARK → REFINE.

Hereafter, we replace the subscript h by k, where k is the counter of the adaptive loop. Then, given a mesh $\mathcal{T}_k$, the procedure SOLVE is a direct solver for computing the discrete solution $(\boldsymbol{\sigma}_k, \mathbf{u}_k)$. ESTIMATE calculates the error indicators η_T (resp., $\tilde{\eta}_T$) for all $T \in \mathcal{T}_k$ depending on the computed solution and the data. Based on the values of $\{\eta_T\}_{T\in\mathcal{T}_k}$ (resp., $\{\tilde{\eta}_T\}_{T\in\mathcal{T}_k}$), the procedure MARK generates a set of marked elements subject to refinement. For the elements selection, we rely on the *maximum* strategy: Given a threshold $\gamma \in (0, 1]$, any element $T' \in \mathcal{T}_k$ with

$$\eta_{T'} > \gamma \max_{T\in\mathcal{T}_k}\eta_T\,, \qquad (\text{resp., } \tilde{\eta}_{T'} > \gamma \max_{T\in\mathcal{T}_k}\tilde{\eta}_T) \tag{53}$$

is marked for refinement. Finally, the procedure REFINE creates a conforming refinement $\mathcal{T}_{k+1}$ of $\mathcal{T}_k$, bisecting d times all marked elements.

We will compare the performance of a finite element method based on uniform refinement (UR) with the adaptive method (AR) that we have described above.

In the examples below, we choose κ_1 and κ_2 as in [1]:

$$\kappa_1 = \frac{\nu}{1+\nu^2+d\|\mathbf{a}\|^2_{[L^\infty(\Omega)]^2}} \qquad \text{and} \qquad \kappa_2 = \frac{\nu\left(1+d\|\mathbf{a}\|^2_{[L^\infty(\Omega)]^2}\right)}{1+\nu^2+d\|\mathbf{a}\|^2_{[L^\infty(\Omega)]^2}}.$$

In what follows, DOFs stand for the total number of degrees of freedom (unknowns) of the discrete scheme (10) and we define the individual errors

$$e_k(\boldsymbol{\sigma}) := \|\boldsymbol{\sigma}-\boldsymbol{\sigma}_k\|_{H(\mathbf{div};\Omega)}\,, \quad e_k(\mathbf{u}) := |\mathbf{u}-\mathbf{u}_k|_{[H^1(\Omega)]^d}\,, \quad e_k(p) := \|p-p_k\|_{L^2(\Omega)},$$

where the pressure p_k is recovered as $p_k = -\frac{1}{d}\mathrm{tr}(\boldsymbol{\sigma}_k)$, and the total error

$$e_k(\boldsymbol{\sigma},\mathbf{u}) := \left(e_k(\boldsymbol{\sigma})^2 + e_k(\mathbf{u})^2\right)^{1/2}.$$

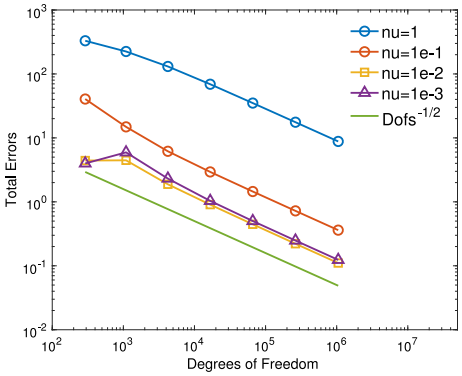

Fig. 1. Example 1: Total error vs. DOFs for different values of ν.

The efficiency index with respect to the error estimator η_k (resp., $\tilde{\eta}_k$) is defined as $\mathrm{eff}_k := e_k(\boldsymbol{\sigma}, \mathbf{u})/\eta_k$ (resp., $\mathrm{eff}_k := e_k(\boldsymbol{\sigma}, \mathbf{u})/\tilde{\eta}_k$).

In the following four subsections we present numerical experiments for the Oseen problem. The aim of Section 6.1 is to confirm the theoretical convergence rates predicted by the theory (see Theorem 3). In Sections 6.2 and 6.3, we consider two examples with a singular solution in order to study the efficiency of the adaptive method. In Section 6.2, we choose a non-convex domain, whereas in Section 6.3, we choose a domain with a crack. Finally, in Section 6.4 we present some results concerning the solution of an Oseen problem in three dimensions.

6.1. Kovasznay flow

We first consider an example with a smooth solution due to Kovasznay [21]. We let $\Omega = (-\frac{1}{2}, \frac{3}{2}) \times (0, 2)$, $\Gamma_N = \{\frac{3}{2}\} \times (0, 2)$ and $\Gamma_D = \Gamma \setminus \Gamma_N$; $\mathbf{a} = (1, 0)^{\mathrm{t}}$ and consider $\nu = 10^{-i}$, for $i = 0, \ldots, 3$. The data are chosen so that the exact solution is

$$\mathbf{u}(x, y) = \begin{pmatrix} 1 - e^{\lambda x}\cos(2\pi y) \\ \dfrac{\lambda}{2\pi} e^{\lambda x}\sin(2\pi y) \end{pmatrix}, \qquad p(x, y) = -\frac{1}{2}e^{2\lambda x}$$

with $\lambda = -\frac{8\pi^2\nu}{1+\sqrt{1+16\pi^2\nu^2}}$.

We solved the problem over a sequence of uniform meshes. In Fig. 1 we show the total error versus the DOFs for different values of ν. We observe that optimal convergence rates are attained in all cases. In Fig. 2 we show the numerical solutions obtained for the different values of ν.

6.2. Non-convex Lipschitz domain

We consider now an academic example inspired by [22]. In this case, $\Omega = \{|x| + |y| < 1\} \cap \{x < 0 \text{ or } y > 0\}$ is a non-convex Lipschitz domain, $\Gamma_D = \{0\} \times (-1, 0) \cap (0, 1) \times \{0\}$ and $\Gamma_N = \Gamma \setminus \Gamma_D$. The advective velocity is $\mathbf{a} = (2, 3)^{\mathrm{t}}$ and the viscosity $\nu = 0.05$. The exact solution in polar coordinates is

$$\mathbf{u}(r, \theta) = r^{\lambda}\begin{pmatrix} (1+\lambda)\sin(\theta)\,\Psi(\theta) + \cos(\theta)\,\Psi'(\theta) \\ \sin(\theta)\,\Psi'(\theta) - (1+\lambda)\cos(\theta)\,\Psi(\theta) \end{pmatrix}, \qquad p(r, \theta) = -\frac{(1+\lambda)^2\,\Psi'(\theta) + \Psi'''(\theta)}{1-\lambda}\,r^{\lambda-1}, \tag{54}$$

where

$$\Psi(\theta) = \frac{\sin((1+\lambda)\theta)\cos(\lambda\omega)}{1+\lambda} - \cos((1+\lambda)\theta) - \frac{\sin((1-\lambda)\theta)\cos(\lambda\omega)}{1-\lambda} + \cos((1-\lambda)\theta),$$

with $\omega = \frac{3\pi}{2}$ and $\lambda \approx 0.54448373\ldots$ being the smallest positive solution of the nonlinear equation

$$\sin(\lambda\omega) + \lambda\sin(\omega) = 0.$$

We emphasize that the exact solution $(\mathbf{u}, p)$ presents singularities at the origin, since $\mathbf{u} \sim r^{\lambda}$ and $p \sim r^{\lambda-1}$.

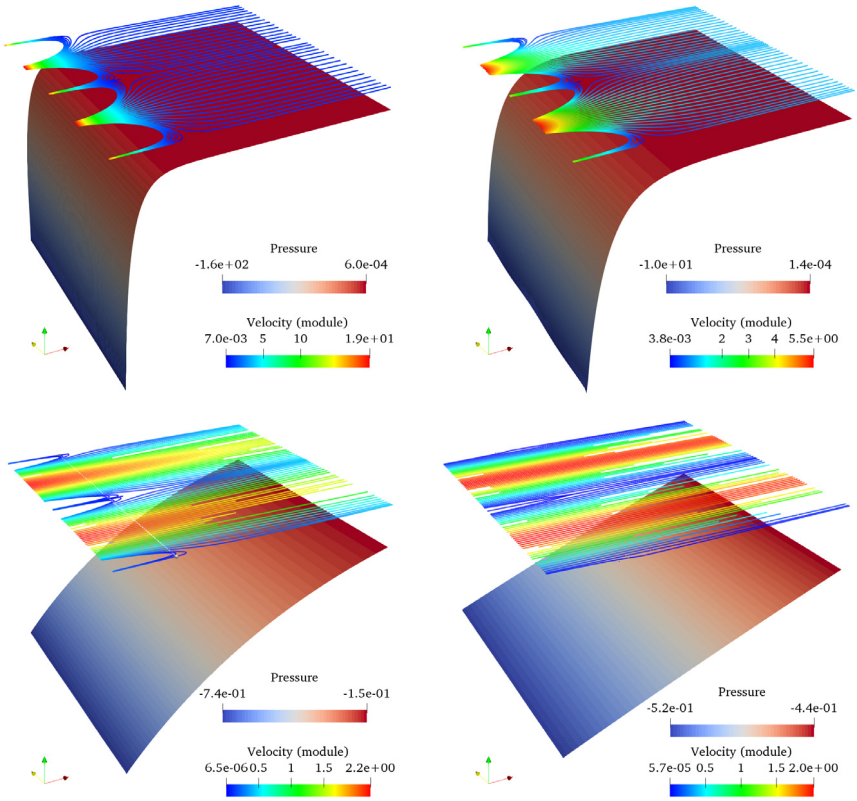

Fig. 2. Example 1: From top-left to botton-right, pressure and velocity module for $\nu = 1, 10^{-1}, 10^{-2}, 10^{-3}$ obtained with uniform refinement (UR) for Kovasznay flow.

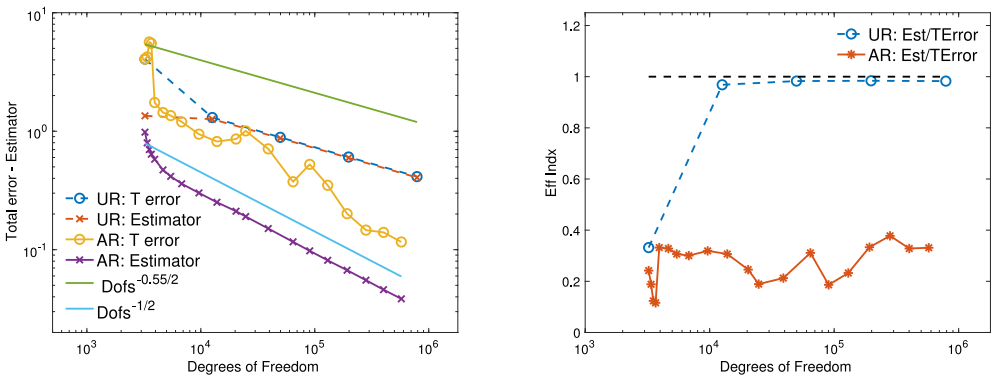

Fig. 3. Example 2: Total error and indicator vs. DOF (left) and efficiency indices vs. DOF (right).

In Fig. 3, we show, on the left, the total error and the indicator values versus the DOFs for the uniform (UR) and adaptive (AR) refinement. In this case, the uniform refinement procedure is not able to attain the optimal convergence rate due to the singularity of the solution at the origin. The convergence graph for the AFEM algorithm is a bit erratic although it seems to approach linear convergence in the final steps. On the right, we show the efficiency indices, that are fairly stable for the uniform refinement and take values between 0.2 and 0.4 for the AFEM algorithm. In Fig. 4 we show the initial mesh and some adapted meshes generated by the AFEM algorithm. We can observe that the meshes are highly refined around the origin, where the pressure presents a singularity. Finally, in Fig. 5 we show the pressure and velocity isolines at different steps of the AFEM algorithm.

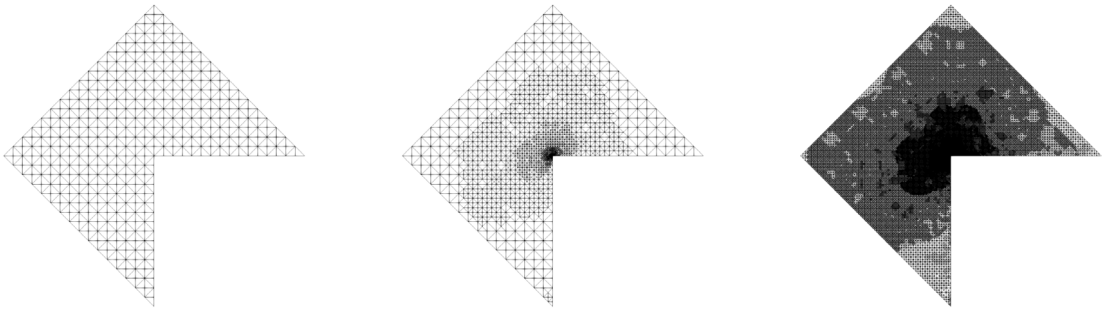

Fig. 4. Example 2: From left to right, initial mesh and meshes at iterations 9 and 18.

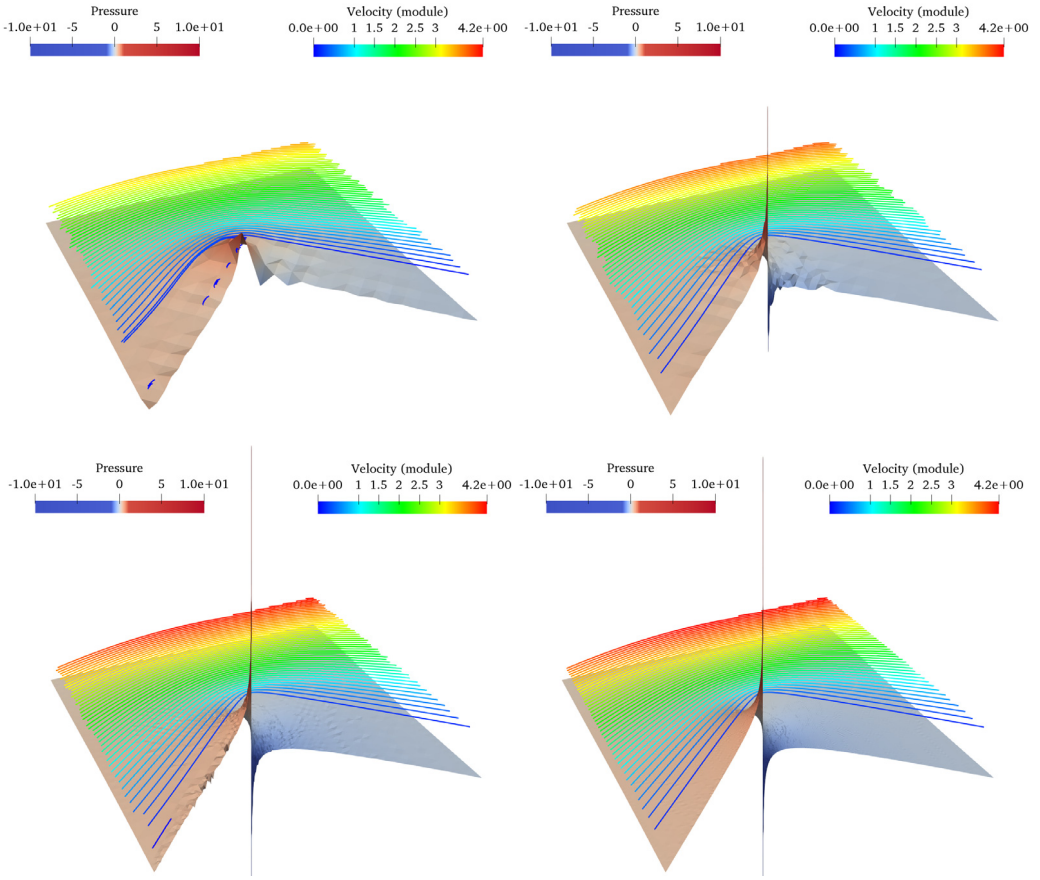

Fig. 5. Example 2: From top-left to bottom-right, pressure and velocity isolines at iterations 0, 6, 12 and 18, respectively.

6.3. A domain with a crack

We consider another academic example inspired by [22]. In this case, the domain $\Omega = \{|x| + |y| < 1\} \setminus \{x \in (0, 1) \text{ and } y = 0\}$ is a non-Lipschitz domain, $\Gamma_D = \{x \in (0, 1) \text{ and } y = 0\}$ and $\Gamma_N = \Gamma \setminus \Gamma_D$. The advective velocity is $\mathbf{a} = (2, 3)^t$ and the viscosity $\nu = 1$. The exact solution in polar coordinates is given by (54), with

$$\Psi(\theta) = 3\ \sin(0.5\,\theta) - \sin(1.5\,\theta)\,, \qquad \lambda = 0.5.$$

We remark that this example is out of the framework of our theory because the domain is non-Lipschitz.

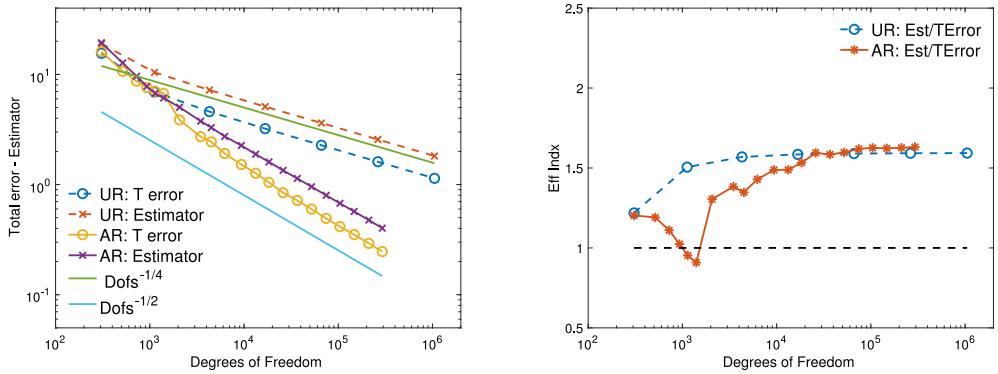

Fig. 6. Example 3: Total error and estimator vs. DOF (left) and efficiency indices vs. DOF (right).

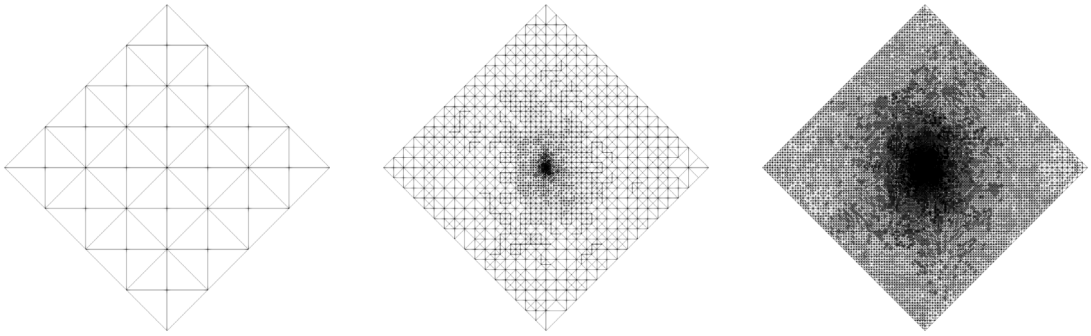

Fig. 7. Example 3: From left to right, initial mesh and meshes at iterations 12 and 20.

In Fig. 6 we show, on the left, the total error and indicator values versus the DOFs for the uniform (UR) and adaptive (AR) refinement. As in the previous example, the uniform refinement is not able to attain the optimal order of convergence, due to the singularity of the solution. The AFEM algorithm, on the other hand, recovers the optimal convergence rate. On the right, we show the efficiency indices, that tend to stabilize around the value 1.5. In Fig. 7, we show the initial mesh, an intermediate mesh and the final mesh. We observe that the refinements concentrate around the origin, where the pressure is singular. Finally, in Fig. 8 we show the pressure and the velocity isolines obtained with different AFEM meshes.

6.4. A three-dimensional example

Let us consider $\Omega = (0,1)\times(0,1)\times(0,1)$, $\Gamma_N = (0,1)\times(0,1)\times\{0\}$ and $\Gamma_D = \partial\Omega \setminus \Gamma_N$, $\mathbf{a} = (1,1,1)^t$ and choose $\mathbf{f}$ and $\mathbf{g}$ so that the exact solution is

$$\mathbf{u}(x,y,x) = \begin{pmatrix} 10y(1-y)z(1-e^{15(z-1)}) \\ x(1-z) \\ x\,y \end{pmatrix} \qquad p(x,y,z) = x\,y\,z.$$

We remark that the solution has a boundary layer around the plane $z = 1$.

In Fig. 9, we show the individual errors (left) and total errors and indicators (right) for the uniform and adaptive refinements. In Fig. 10, we show the efficiency indices for both refinements. Finally, in Fig. 11 we show the velocity module on the half domain $(0,\frac{1}{2})\times(0,1)\times(0,1)$ for different iterations of the adaptive algorithm.

7. Conclusions

We propose new mixed finite element methods for the Oseen problem with mixed boundary conditions in the pseudostress-velocity variables. We prove that for appropriate values of the stabilization parameters, the discrete

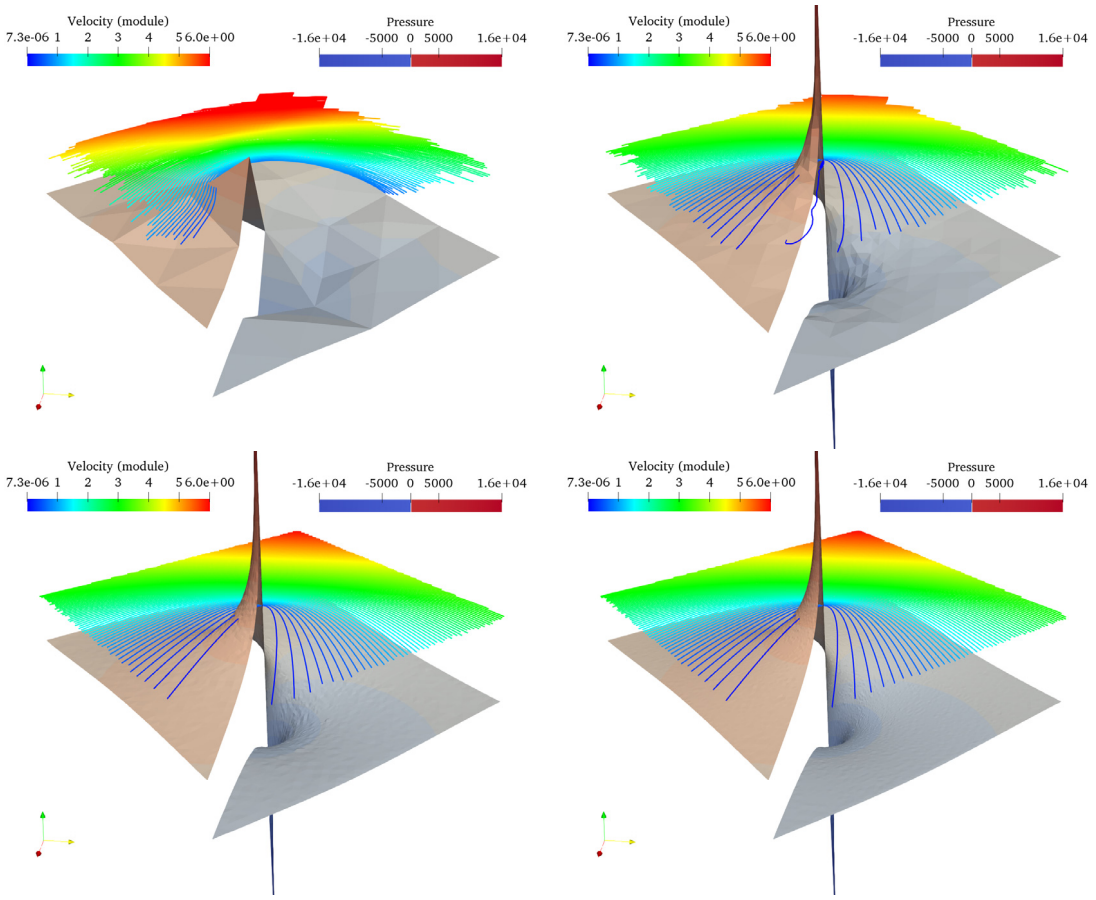

Fig. 8. Example 3: Pressure and velocity isolines at iterations 0, 8, 16 and 20, respectively.

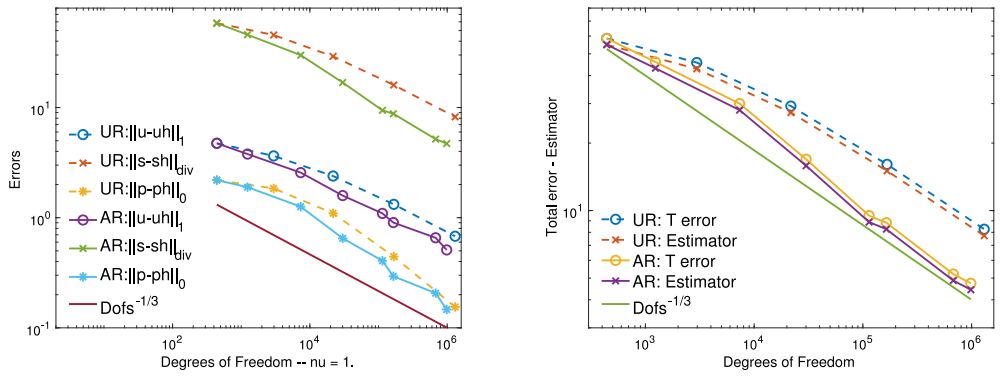

Fig. 9. Example 4: Individual errors (left) and total errors and indicators (right) for uniform and adaptive refinements.

schemes are well-posed and optimal error estimates hold when the solution is sufficiently smooth. Moreover, we developed a residual-based a posteriori error analysis based on a quasi-Helmholtz decomposition in two dimensions and a Helmholtz decomposition in three dimensions, and obtain simple a posteriori error indicators that are reliable and locally efficient. Finally, we show the performance of the method through some numerical experiments.

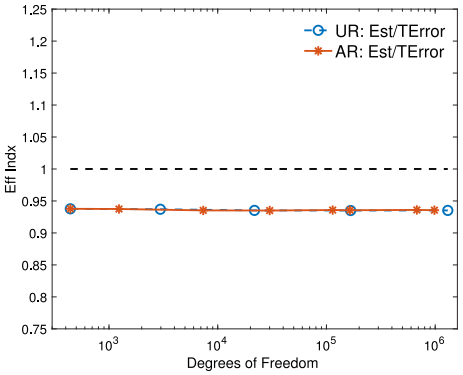

Fig. 10. Example 3: Efficiency indices for uniform and adaptive refinements.

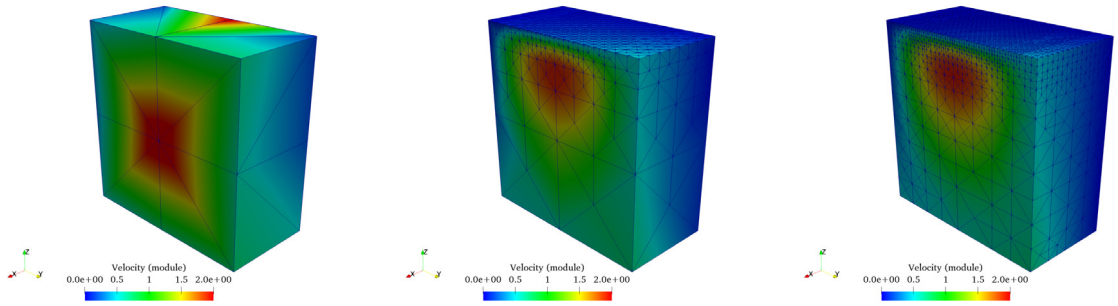

Fig. 11. Example 3: Velocity module on half domain for iterations 0 (left), 4 (center) and 7 (right).

Declaration of competing interest

The authors declare that they have no known competing financial interests or personal relationships that could have appeared to influence the work reported in this paper.

Acknowledgments

The authors acknowledge the support of CITIC. CITIC, as a Research Center of the Galician universitary system is financed by Consellería de Educación, Universidade e Formación Profesional da Xunta de Galicia through Fondo Europeo de Desenvolvemento Rexional (FEDER) at 80%, operative program FEDER Galicia 2014–2020 and at the remaining 20% from Secretaría Xeral de Universidades (grant ED431G 2019/01). Moreover, the research of T.P.B. is partially supported by Dirección de Investigación of the Universidad Católica de la Santísima Concepción (Chile) and through CONICYT-Chile FONDECYT project 1160578. The research of M.G. is partially supported by the Spanish Ministerio de Economía y Competitividad Grant MTM2016-76497-R, by Ministerio de Ciencia, Innovación y Universidades, Spain grant PRX19/00475, by Xunta de Galicia, Spain through Grant GRC ED431C 2018-033 and by CITIC, Spain.

References

[1] T.P. Barrios, J.M. Cascón, M. González, Augmented mixed finite element method for the Oseen problem: A priori and a posteriori error analyses, Comput. Methods Appl. Mech. Engrg. 313 (2017) 216–238.

[2] T.P. Barrios, E.M. Behrens, M. González, Low cost a posteriori error estimators for an augmented mixed FEM in linear elasticity, Appl. Numer. Math. 84 (2014) 46–65.

[3] T.P. Barrios, J.M. Cascón, M. González, A posteriori error analysis of an augmented mixed finite element method for Darcy flow, Comput. Methods Appl. Mech. Engrg. 283 (2015) 909–922.

[4] A. Masud, T.J.R. Hughes, A stabilized mixed finite element method for Darcy flow, Comput. Methods Appl. Mech. Engrg. 191 (2002) 4341–4370.

[5] L. Figueroa, G.N. Gatica, A. Márquez, Augmented mixed finite element methods for the stationary Stokes equations, SIAM J. Sci. Comput. 31 (2) (2008) 1082–1119.
[6] M. González, Stabilized dual-mixed method for the problem of linear elasticity with mixed boundary conditions, Appl. Math. Lett. 30 (2014) 1–5.
[7] T.P. Barrios, R. Bustinza, G.C. García, E. Hernández, On stabilized mixed methods for generalized Stokes problem based on the velocity-pseudostress formulation: A priori error estimates, Comput. Methods Appl. Mech. Engrg. 237–240 (2012) 78–87.
[8] M. González, J. Jansson, S. Korotov, A posteriori error analysis of a stabilized mixed FEM for convection–diffusion problems, Discrete Contin. Dyn. Syst. (2015) 525–532, Dynamical systems, differential equations and applications. 10th AIMS Conference. Suppl..
[9] Z. Cai, C. Tong, P. Vassilevski, C. Wang, Mixed finite element methods for incompressible flow: stationary Stokes equations, Numer. Methods Partial Differential Equations 26 (4) (2010) 957–978.
[10] J.M. Cascón, R.H. Nochetto, K.G. Siebert, Design and convergence of AFEM in H(DIV), Math. Models Methods Appl. Sci. 17 (11) (2007) 1849–1881.
[11] T.P. Barrios, R. Bustinza, G.C. García, M. González, A posteriori error analyses of a velocity-pseudostress formulation of the generalized Stokes problem, J. Comput. Appl. Math. 357 (2019) 349–365.
[12] G.N. Gatica, A note on stable Helmholtz decompositions in 3D, Appl. Anal. (2018) http://dx.doi.org/10.1080/00036811.2018.1522627 (in press).
[13] F. Brezzi, M. Fortin, Mixed and Hybrid Finite Element Methods, Springer-Verlag, 1991.
[14] D.N. Arnold, J. Douglas, Ch.P. Gupta, A family of higher order mixed finite element methods for plane elasticity, Numer. Math. 45 (1984) 122.
[15] J.E. Roberts, J.-M. Thomas, Mixed and hybrid methods, in: P.G. Ciarlet, J.L. Lions (Eds.), Handbook of Numerical Analysis, in: Finite Element Methods (Part 1), vol. II, North-Holland, Amsterdam, 1991.
[16] P. Clément, Approximation by finite element functions using local regularisation, RAIRO Modél. Math. Anal. Numér. 9 (1975) 77–84.
[17] P.G. Ciarlet, The Finite Element Method for Elliptic Problems, North-Holland, 1978.
[18] S. Agmon, Lectures on Elliptic Boundary Value Problems, Van Nostrand, Princeton, New Jersey, 1965.
[19] R. Verfürth, A posteriori error estimates for nonlinear problems. Finite element discretizations of elliptic equations, Math. Comp. 62 (206) (1994) 445–475.
[20] A. Schmidt, K.G. Siebert, Design of Adaptive Finite Element Software: The Finite Element Toolbox ALBERTA, in: LNCSE, vol. 42, Springer, 2005.
[21] L.I.G. Kovasznay, Laminar flow behind a two-dimensional grid, Proc. Cambridge Philos. Soc. 44 (1948) 5862.
[22] R. Verfürth, A Review of a Posteriori Error Estimation and Adaptive Mesh-Refinement Techniques, Wiley-Teubner, Chichester, 1996.